



**HAL**  
open science

## Disordered information processing dynamics in experimental epilepsy

Wesley Clawson, Tanguy Madec, Antoine Ghestem, Pascale Quilichini,  
Demian Battaglia, Christophe Bernard

► **To cite this version:**

Wesley Clawson, Tanguy Madec, Antoine Ghestem, Pascale Quilichini, Demian Battaglia, et al..  
Disordered information processing dynamics in experimental epilepsy. 2021. hal-03437593

**HAL Id: hal-03437593**

**<https://hal.science/hal-03437593>**

Preprint submitted on 20 Nov 2021

**HAL** is a multi-disciplinary open access archive for the deposit and dissemination of scientific research documents, whether they are published or not. The documents may come from teaching and research institutions in France or abroad, or from public or private research centers.

L'archive ouverte pluridisciplinaire **HAL**, est destinée au dépôt et à la diffusion de documents scientifiques de niveau recherche, publiés ou non, émanant des établissements d'enseignement et de recherche français ou étrangers, des laboratoires publics ou privés.

# 1 Disordered information processing dynamics in experimental epilepsy

2 Wesley Clawson<sup>1</sup>, Tanguy Madec<sup>1</sup>, Antoine Ghestem<sup>1</sup>, Pascale P Quilichini<sup>1,\*</sup>, Demian

3 Battaglia<sup>1,\*</sup>, Christophe Bernard<sup>1,\*</sup>

4 1. Aix Marseille Univ, Inserm, INS, Institut de Neurosciences des Systèmes, Marseille, France

5 \* - Equally contributing last authors

6

## 7 Abstract

8 Neurological disorders share common high-level alterations, such as cognitive deficits, anxiety,  
9 and depression. This raises the possibility of fundamental alterations in the way information  
10 conveyed by neural firing is maintained and dispatched in the diseased brain. Using  
11 experimental epilepsy as a model of neurological disorder we tested the hypothesis of altered  
12 information processing, analyzing how neurons in the hippocampus and the entorhinal cortex  
13 store and exchange information during slow and theta oscillations. We equate the storage and  
14 sharing of information to low level, or primitive, information processing at the algorithmic level,  
15 the theoretical intermediate level between structure and function. We find that these low-level  
16 processes are organized into substates during brain states marked by theta and slow  
17 oscillations. Their internal composition and organization through time are disrupted in epilepsy,  
18 losing brain state-specificity, and shifting towards a regime of disorder in a brain region  
19 dependent manner. We propose that the alteration of information processing at an algorithmic  
20 level may be a mechanism behind the emergent and widespread co-morbidities associated with  
21 epilepsy, and perhaps other disorders.

## 22 Introduction

23 Most, if not all, neurological pathologies, including Alzheimer's disease, epilepsies, and  
24 Parkinson's disease, aside from their specificities, display commonalities in terms of cognitive  
25 (e.g., memory) and mental (e.g., anxiety and depression) disorders (Hesdorffer, 2016).  
26 Historically, attempts have been made to correlate higher-level changes to the underlying  
27 structural alterations. However, structural alterations may be very different from one pathology  
28 to the next, even within a given brain disorder. The origin of shared and generic deficits must  
29 therefore be sought for at a level higher than the structural one. We hypothesize that diverse  
30 pathological mechanisms can lead to similar modifications of information processing, emerging  
31 from, and existing between, structural and functional levels. Whether information processing is  
32 modified in a pathological context is not known. Furthermore, a formal framework for the  
33 quantification of these processes is missing.

34

35 As a model of neurological disorder, we consider Temporal Lobe Epilepsy (TLE), the most  
36 common form of epilepsy in adults (Tatum, 2012). TLE is itself highly heterogenous in terms of  
37 differences of histopathology (Blumcke et al., 2013), semiology (Barba et al., 2007; Bartolomei et  
38 al., 2008) and cognition and mental state (de Barros Lourenco et al., 2020; Holmes, 2015;  
39 Krishnan, 2020). Such heterogeneity is also found in experimental models of TLE (Rusina et al.,  
40 2021). Structural alterations may change several features that are relevant for information  
41 processing, such as rate coding, temporal coding, synaptic plasticity, and network oscillations  
42 (Lenck-Santini & Scott, 2015). In keeping with this proposal, hippocampal place cells are unstable,  
43 firing becomes randomized during ripples, synaptic plasticity, and oscillations are altered, and

44 these changes are correlated with deficits in hippocampus-dependent spatial memory in  
45 experimental epilepsy (Chauvière et al., 2009; Inostroza et al., 2013; Lenck-Santini & Holmes,  
46 2008; Lopez-Pigozzi et al., 2016; Suarez et al., 2012; Valero et al., 2017). Given this diversity of  
47 deficits, it is reasonable to presume that in TLE local information processing is altered at a more  
48 fundamental level, with widespread impacts on multiple functions.

49

50 It is difficult to link specific alterations at the structural level to high order cognitive deficits as we  
51 do not know where information processing is localized, what is being processed, nor how it is  
52 integrated into function. In other words, with reference to the notion of the *algorithmic* level  
53 introduced by Marr and Poggio (1977), we do not know what are the “algorithms” that bridge  
54 structure and function. The common axiomatic view is that neural information processing stems  
55 from the spatiotemporal organization of the firing of neurons. Information theory was designed  
56 to be agnostic to the content of information and thus provides useful metrics to track primitive,  
57 or fundamental, information processing operations (Shannon, 1948). Neuronal firing intrinsically  
58 carries information due to its statistical properties. Auto-correlations in firing actively maintain  
59 this information through time - active information *storage* (Lizier et al., 2012; Wibral et al., 2014),  
60 and cross-correlated firing between different neurons allows the sharing of this information  
61 between themselves (Kirst et al., 2016). Focusing on such basic operations allows investigation  
62 of how patterns of coordinated neural firing may translate into primitive low-level information  
63 processing (Clawson et al., 2019), akin to the algorithmic level. Here, we hypothesize that the key  
64 differences between control and epileptic networks are not only present at the structural level,  
65 but also at a more general and core algorithmic level of quantifiable primitive operations.

66

67 To test this hypothesis, a multilevel experimental approach is required (Scott et al., 2018). Multi-  
68 channel electrode recordings of neural populations provide such a dataset which spans two levels  
69 of analysis: the action potential at the neuronal level and oscillations at the population level. As  
70 neural computation is brain state dependent (Quilichini & Bernard, 2012), we consider the global  
71 brain states of theta (THE) and slow oscillations (SO), which can be recorded during anesthesia.  
72 Previous work in control animals demonstrate that neuronal activity patterns in the hippocampus  
73 and entorhinal cortex switch between different information processing substates (IPSs) (Clawson  
74 et al., 2019). An IPS corresponds to an epoch in which primitive operations of information storage  
75 and sharing in a local microcircuit remain temporally consistent. IPSs continuously switch from  
76 one IPS to another, similarly to what has been described at higher level of organization, such as  
77 the dynamics of resting state networks and EEG microstates (Calhoun et al., 2014; Van de Ville et  
78 al., 2010). In the control hippocampus and entorhinal cortex, the sequences of IPSs are complex,  
79 i.e. standing between order and disorder (Clawson et al., 2019).

80

81 Using an unbiased quantification of IPSs, we compare their properties and organization between  
82 control and experimental epilepsy conditions. We focus on the hippocampus and the entorhinal  
83 cortex, two major structures commonly affected in TLE (Curia et al., 2008). We find that IPS'  
84 internal organization and switching dynamics, although not suppressed, shift toward a less  
85 structured and more random spatiotemporal organization in experimental epilepsy than in  
86 control. Such disruption of information processing at the algorithmic level itself could underly the  
87 general performance impairments in TLE.

## 88 Results

### 89 Design

90 We analyze the local field potentials (LFPs) and action potentials from individual neurons  
91 measured in the hippocampus (CA1) and medial entorhinal cortex (mEC) from control (n = 5) and  
92 experimental epilepsy (n = 6) rats under anesthesia (Figure 1A-B, see Methods for details).  
93 Unsupervised clustering of the spectral content of LFPs reveals that field activity continuously  
94 switches between two states: slow oscillations (SO, 0.5-3 Hz) and theta oscillations (THE, 3-6 Hz)  
95 (Figure 1B, S1). As previously reported in freely moving animals (Chauvière et al., 2009), THE  
96 power and peak frequency are decreased in CA1 in experimental epilepsy (Figure S1). Although,  
97 the peak frequencies of THE and SO are not modified in the mEC in epilepsy, their power is  
98 decreased (Figure S1). However, both frequency and power ratios between SO and THE are  
99 similar in control and epilepsy.

100

101 We extract three features from the spike trains using a sliding widow procedure (Figure 1B-C):  
102 (1) firing, the number of times a neuron fired within a window, (2) storage, the information  
103 theoretical measure of active information storage (Lizier et al., 2012; Wibral et al., 2014), which  
104 captures temporal patterns of spiking for a single neuron within a window – notably in our case,  
105 how regular or repetitive these patterns are – and (3) sharing, an information theoretical  
106 measure of information sharing (Kirst et al., 2016), which captures spatiotemporal patterns of  
107 coordinated spiking across neurons within a window. First, we examine whether these features  
108 are dependent upon the brain state (THE versus SO), the region (CA1 versus mEC) and the  
109 condition (control versus epilepsy).

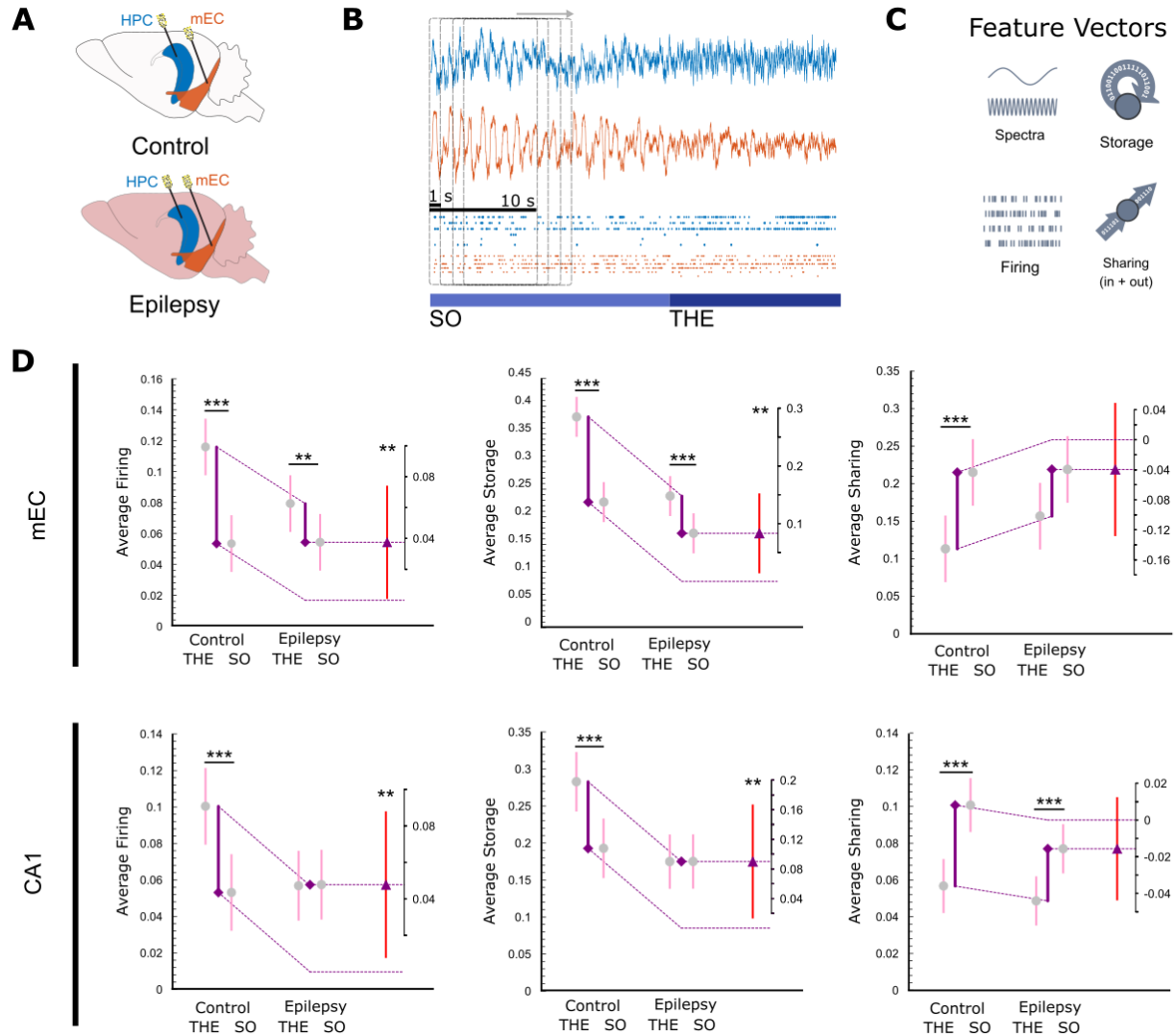
110 **Epilepsy reduces firing, storage and sharing differences between THE and SO states**

111 In control animals, we find that in both regions, average firing and storage of all neurons is larger  
112 during THE than SO, while average sharing is lower (Figure 1D, see also S2), in keeping with the  
113 idea that neuronal computation is brain state-dependent (Quilichini & Bernard, 2012). In  
114 epilepsy, we find that average firing and storage are decreased during THE, but not during SO, as  
115 compared to control in both mEC and HPC. As a consequence, the brain state-dependency of  
116 firing and storage, which is consistent across controls, is reduced in both regions in epilepsy  
117 (Figure 1D). There is thus, in epilepsy, a large deviation from the operating mode found in control  
118 conditions.

119

120 We have previously shown that THE and SO states are in fact characterized by a complex dynamic  
121 organization in terms of firing, storage or sharing features (Clawson et al., 2019). A feature value  
122 (e.g., storage) can remain stable during a given time period (i.e., during successive windows),  
123 before switching to a different feature value with its own period of stability. We called these  
124 periods of stability *substates* of firing, storage or sharing. We begin by assessing the properties  
125 of substates in control and in epilepsy, as substate switching constitutes an important qualitative  
126 aspect of coordinated firing dynamics.

127



128

129

130 **Figure 1: Experimental and analytical design** - (A) Cartoon representing the approximate recording

131 locations in mEC (orange) and CA1 (blue) in control and experimental epilepsy. (B) Example of LFP (top)

132 and firing (bottom, each line represents one neuron, a dot represents an action potential) data recorded

133 in control CA1 and mEC during SO and THE. Overlaid is a representation of our analytic method that

134 uses 10 s long sliding windows shifted by 1 s at each step. (C) Cartoon examples of the four acquired

135 data features. (D) Average values and difference of differences graphs for data features taken from

136 spiking data during epochs of THE and SO in mEC (top) and CA1 (bottom) in both control and epilepsy



137 conditions. See S2 for the same graph represented as a function of region, rather than oscillatory state.  
138 Circles and triangles represent the mean, and all bars represent a 99% bootstrapped confidence interval.  
139 Significance is shown using the symbol (\*) with their standard corresponding meaning (\*,  $p < 0.05$ ; \*\*,  
140  $p < 0.01$ ; \*\*\*,  $p < 0.001$ ). The numerical values are provided in Table S1.

141

## 142 **Terminology, metrics, and methodology**

143 Figure 2A illustrates an example of the procedure for a ~ 25 min long recording performed in the  
144 mEC in a control animal. Spectral analysis of the LFP reveals the alternation between THE and SO  
145 states (upper row). Through an unsupervised substate extraction procedure based on *k*-means  
146 clustering (see *Methods*), we identify in this example 4, 3, and 5 substates of stable patterns for  
147 firing, storage and sharing, respectively. The four features together, seen as 4 rows in Fig 2A,  
148 define a *switching table*. Each time point in the table corresponds to an *information processing*  
149 *state* (IPS), i.e. a combination of global state, firing rate, storage, and sharing patterns at this time  
150 point. By characterizing which neurons fire, how much, and with which correlation properties, an  
151 IPS provides a robust characterization of the pattern of coordinated activity occurring within each  
152 temporal window. Note that the switching transitions from one substate to the next are not  
153 necessarily synchronous between the different features, a property found in all recordings. In  
154 Figure 2B, we show, encoded as vertical color bars, the absolute values of firing, storage and  
155 sharing features that different neurons assume in the different substates. For a given feature,  
156 the values appear clearly different for a given neuron between substates. We will quantify these  
157 differences in the next section.

158

159 The switching table of Figure 2A is constructed using an unsupervised clustering algorithm,  $k$ -  
160 means, guided by an a priori assumption that (1) there exist separable clusters of data and (2)  
161 there are exactly  $k$  of these clusters (here 4, 3, and 5 for firing, storage and sharing, respectively).  
162 Using a null model, we demonstrate that there exist separable clusters (Figure S3). However, as  
163 the ground truth of how many clusters exist is unknown, statistical criteria can be used to find  
164 the optimal number (as done in Clawson et al., 2019). Here, we use a more general approach  
165 varying the  $k$  value for each firing, storage, and sharing feature while fixing  $k = 2$  for the spectral  
166 feature. Each quadruplet of  $k$  values will produce a specific switching table. Figure 2C illustrates  
167 this concept, showing the resultant clustering of storage substates through time as  $k$  increases  
168 from 3 to 10. A low value may underestimate the real number of substates, while a large number  
169 may be an overestimate producing substates that rarely occur more than once (see Methods).  
170 We therefore use a lower bound of  $k = 3$ , and a reasonable upper bound of  $k = 10$ , wherein the  
171 clusters become too fine (Figure 2C, see Methods). We thus consider eight possible  $k$  values for  
172 each feature, giving rise to  $8^3 = 512$  possible switching tables. Each switching table is  
173 characterized by the total number of substates it contains:  $k_{tot} = 2 + k_{firing} + k_{storage} + k_{sharing}$  with a  
174 maximum value of  $k_{max} = 32$  ( $32 = 2$ , the number of spectral states + 3 features x 10). The  
175 collection of all switching tables for a given recording defines a *library* of tables (Figure 2D). We  
176 chose such a method with the intention that without an a priori approach on the underlying  
177 principle, if we extract generic rules, they should be valid independently of the choice of number  
178 of clusters, at least for a reasonable wide range of  $k$  values. Now, all analysis that can be done on  
179 a switching table is performed for each library, which gives the added benefit of assessing the  
180 robustness of the results regarding the number of clusters.

181

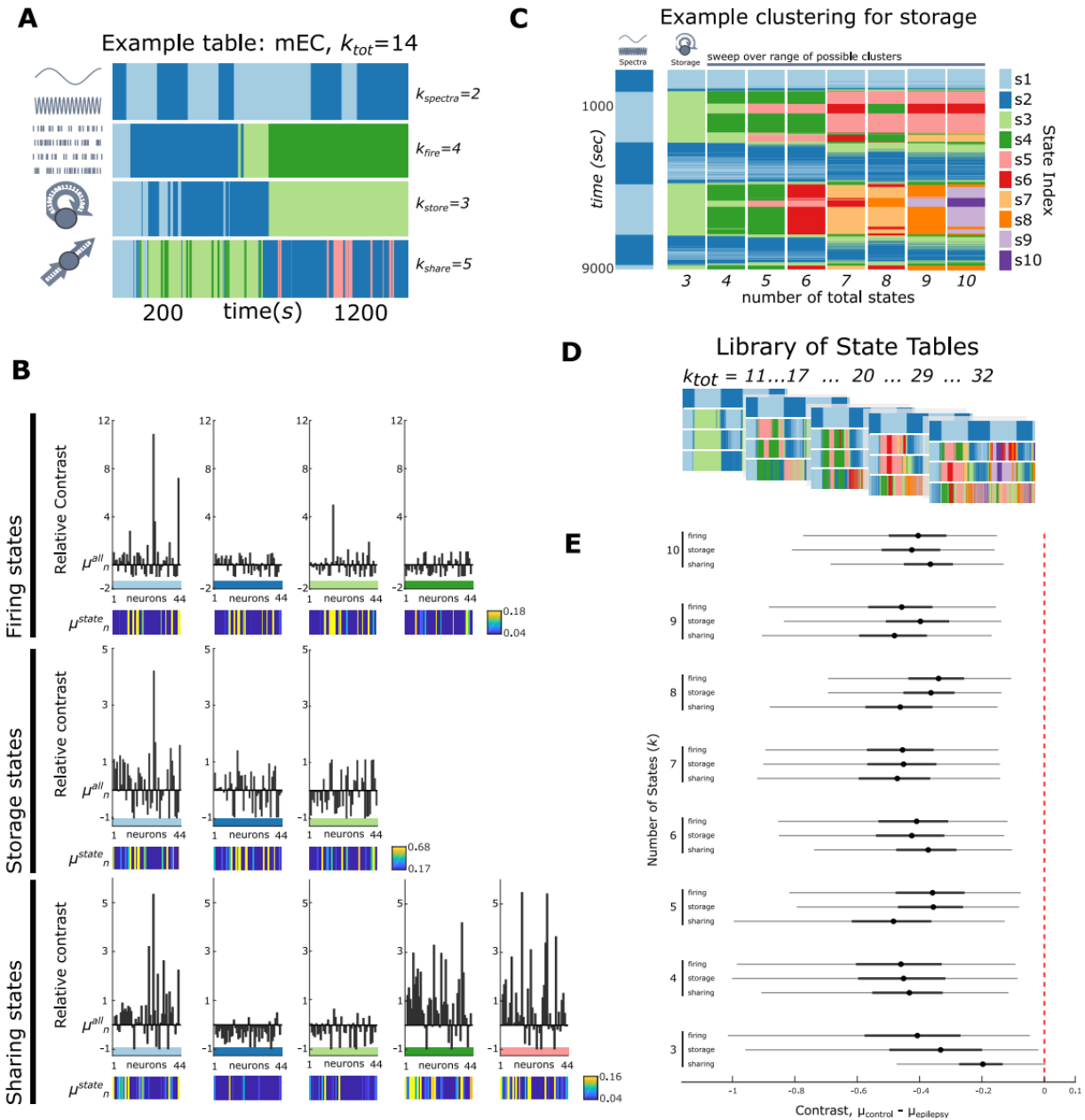
## 182 **Substates are more contrasted in epilepsy**

183 The vertical color bars in Figure 2B qualitatively show that individual neurons can take different  
184 firing, storage or sharing values across substates. In order to quantify these differences, we  
185 measure how “contrasted” are different substates. If we consider the firing feature of a given  
186 neuron, we first calculate its global mean firing rate (over the whole duration of the recording),  
187 and its mean firing rate within each substate. The relative contrast is defined as the difference  
188 between the substate mean firing rate and the global mean firing rate, normalized by the global  
189 mean firing rate. Evaluating contrast allows better tracking of the differing compositions of  
190 substates at the single neuron level. Figure 2B shows the relative contrast plots for the 44  
191 recorded neurons and the various substates in the same dataset and substate decomposition we  
192 use as an example in Figure 2A. The differences between substates for each feature now clearly  
193 appear as large changes in the distributions of contrast values for the recorded neurons. Now,  
194 we extract the *substate contrast* of each substate for each feature - the average of the absolute  
195 values of the heights of the bars in the relative contrast plot. This substate contrast tells us how  
196 much a given substate stands out from its feature’s global average. Increasing the number of  $k$   
197 substates may decrease the substate contrast.

198

199 Figure 2E shows the distributions of the differences in contrasts between control ( $n=5$ ) and  
200 epilepsy ( $n=6$ ), for firing, storage, and sharing features in the mEC, for the chosen  $k$  values  
201 ( $3 \leq k_{firing}, k_{storage}, k_{sharing} \leq 10$ ). For all values of  $k$ , for all features, the contrast differences lie  
202 entirely below zero, demonstrating that substate contrast is generally higher in epilepsy than in

203 control. We also see no clear dependence upon  $k$  values, i.e., the number of substates. The same  
204 result is found in CA1, however higher bounds closer to the 99<sup>th</sup> percentile do cross 0 (Fig S4).  
205 We thus identify another major alteration in epilepsy; substates are more contrasted, exhibiting  
206 more marked differences with respect to the mean. This suggest that in epilepsy, substate  
207 switching more strongly modulates the neural population with regards to firing, storage and  
208 sharing. While this seems to stand in contrast with the previously described reduction of the  
209 modulatory influence exerted by global oscillatory states, this may be explained by a disrupted  
210 articulation between substate and global state, as we explain in the following section.



211

212 **Figure 2 – Clustering & contrast in control and epilepsy –** (A) An example state table for the mEC

213 in a control animal with a total state count of  $k_{tot} = 14$ . The different substates are color coded.

214 Note that switching is not synchronized across the different features. (B) Relative contrast values

215 for the table given shown in (A). The substates shown in A are shown in B as a horizontal bar with

216 the same color. Each graph shows the relative contrast of each of the 44 neurons, for each

217 substate, and each feature. Below each graph is a visual indicator of a neuron’s feature values

218 within the substate (vertical color bar). Here, the color scale varies from near 0, dark blue, to the  
219 top 10% of all average activity within the state. Therefore, any neuron whose activity is within  
220 this top 10% will be bright yellow. (C) Temporal dynamics (vertical axis) of storage substates as a  
221 function of  $k$  (horizontal axis). The far-left column shows the dynamics of THE and SO spectral  
222 states. (D) An example of a resulting state table library, or a collection of all possible combinations  
223 of all clustering with a range of  $k_{tot} = 11 - 32$ . (E) Average contrast difference between control  
224 and epilepsy is shown with respect to both feature and number of states,  $k$ . The circles represent  
225 the mean difference, the thick black bars represent the 25-75% quantile and the thin black bars  
226 represent the 1-99% quantile. The red dotted line is to add the null hypothesis line of no  
227 significant difference between control and epilepsy.

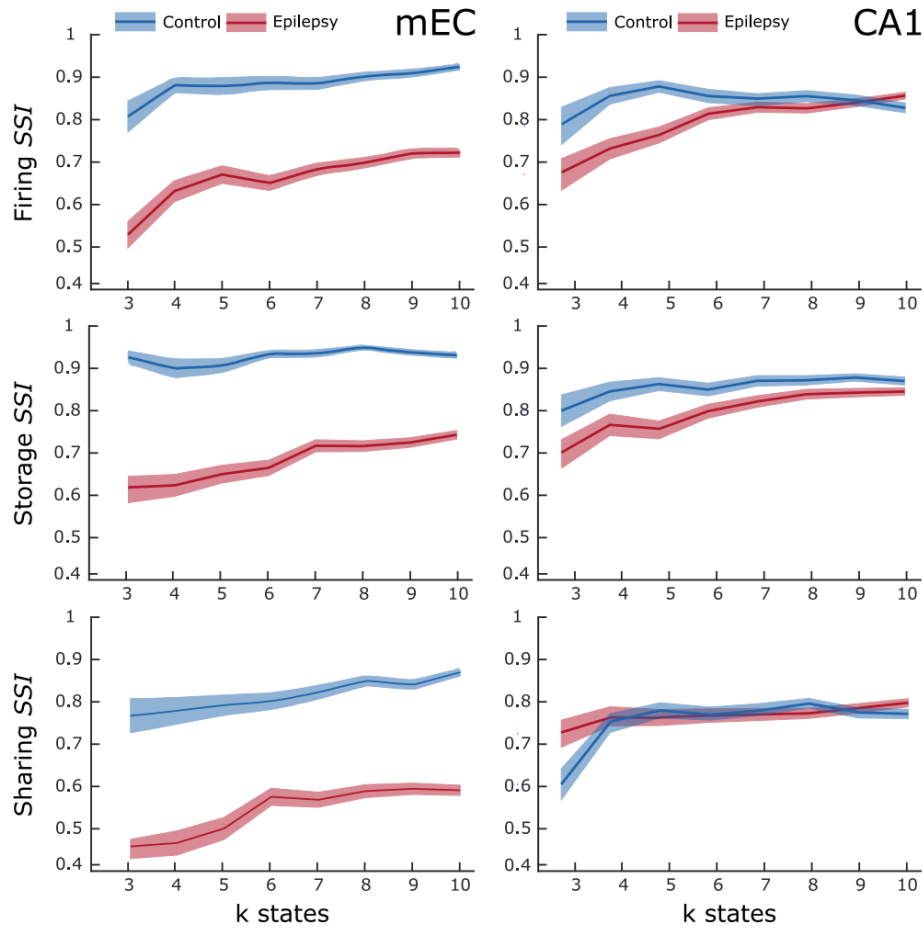
228

### 229 **Loss of global state specificity of firing, sharing and storage substates in epilepsy**

230 Since firing patterns are brain state-dependent, we assess whether this type of specificity is also  
231 found at the level of information processing substates. For a given state table in a library, we  
232 calculate the probability that a substate occurs during THE, SO or both. We name it *state*  
233 *specificity index* (SSI), a metric bounded between 0 (a substate occurs equally in THE or SO) and  
234 1 (a substate is exclusive to either THE or SO) (see Methods). In control animals (Figure 3, blue  
235 curves), most substates are brain state specific in both mEC and CA1, independently of  $k$ . Most  
236 SSI values are above 0.8, well above the null hypothesis  $0.23 \pm 0.03$  value of lack of global state  
237 specificity. Global state specificity of substates is thus a robust result in control animals with  
238 respect to  $k$ .

239 The same analysis performed in epilepsy reveals a region dependent alteration in SSI (Figure 3,  
240 red curves). There is a large decrease in SSI for all features in the mEC, indicating a loss of the  
241 constraint exerted by global oscillatory states on the selection of possible substates, again  
242 regardless to the chosen  $k$ 's. In contrast, there is no such large loss of brain state specificity in  
243 CA1, in particular no change for sharing. We conclude that the substate distribution becomes  
244 “disordered”, i.e., a large proportion of substates now occur during both THE and SO in the mEC  
245 in epilepsy. In contrast, CA1 retains the brain state specificity of the distribution of substates. The  
246 alteration of brain state-specificity of firing, sharing and storage substates is therefore brain  
247 region dependent in epilepsy.

248



249

250 **Figure 3 – Loss of brain state-dependency of substates in the mEC in epilepsy – State similarity**

251 index (SSI) is shown here vs number of  $k$  states for each feature in mEC and CA1. Blue represents

252 the control data while red represents epilepsy. The bold lines represent the mean while the

253 shaded regions represent a 99% bootstrapped confidence interval. The bootstrapped null model

254 produced via randomizing gives an average SSI of  $0.23 \pm 0.03$  and is not shown here to increase

255 visual clarity.



256

257 **Computing hubs are more numerous but less substate-specific in the mEC in epilepsy**

258 Within each substate/feature we extract computing hub neurons, i.e., neurons with on average,  
259 exceptionally high firing, storage or sharing values with regard to the substate (see Methods). As  
260 previously discussed in Clawson et al. (2019), it is important to stress that different substates are  
261 associated to different sets of hubs and that a neuron acting as firing, storage or sharing hub in a  
262 given substate will not necessarily do so in another substate. So, while the fraction of neurons  
263 being hub in a given substate remains small, the fraction of neurons serving as hub at least in one  
264 substate is much larger, approaching ~40% on average. Figure 4A illustrates an example of the  
265 distribution of hubs (same recording as in Figure 2A).

266

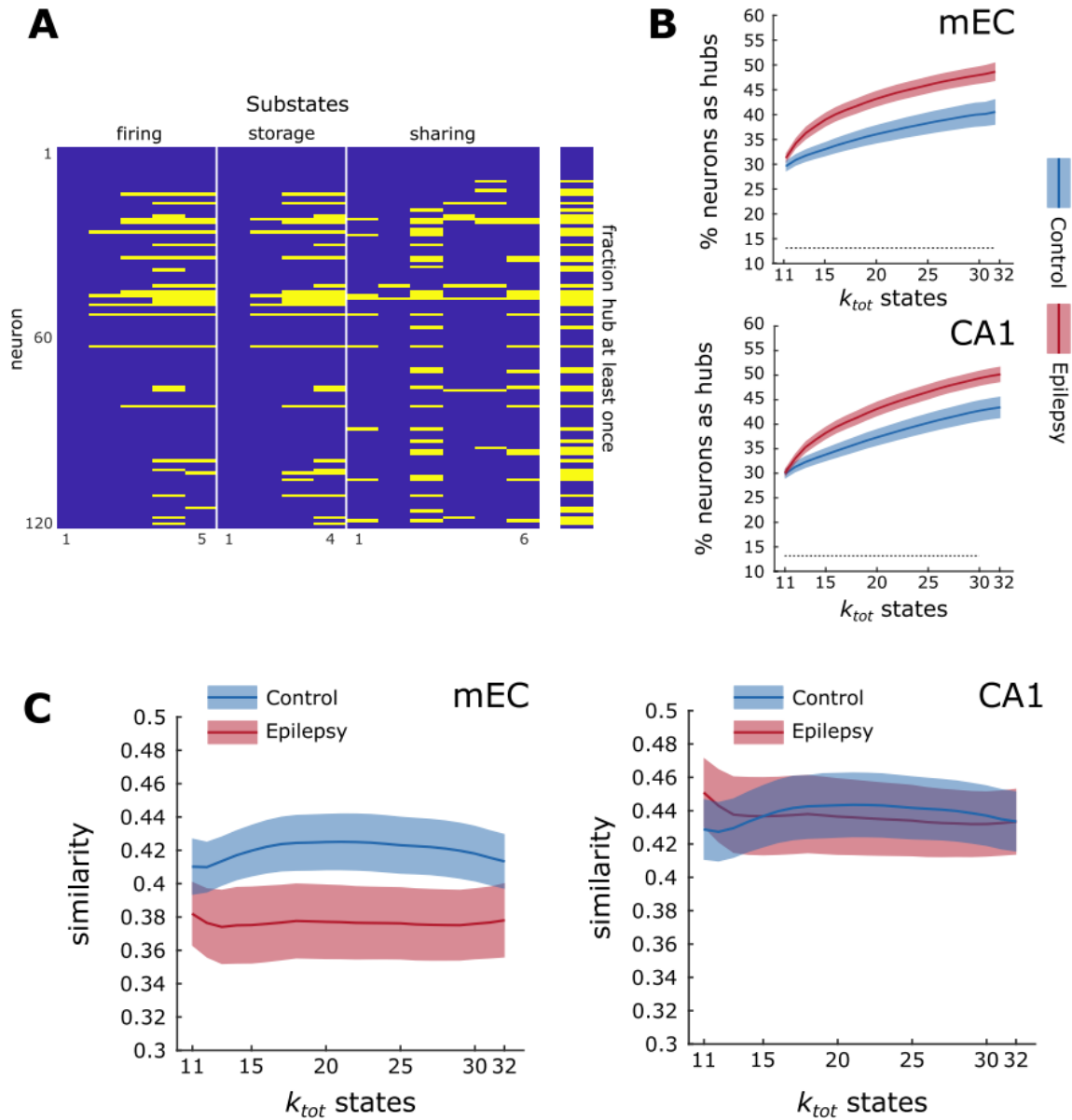
267 In control animals, the percentage of hubs increases with  $k_{tot}$  in both mEC and CA1 (Figure 4B),  
268 which is expected due to the arbitrary over-clustering as  $k$  increases. We observe furthermore  
269 that the percentage of neurons serving as hubs at least once is significantly increased in epilepsy,  
270 by 5% in the mEC and 2.5% in CA1 (Figure 4B). This result is in agreement with the increase in  
271 substate contrast found in epilepsy: more neurons are more contrasted and therefore are  
272 detected as hubs. Note that, for both control and epilepsy, the percentage of neurons marked as  
273 hubs is significantly larger as compared to randomized state tables (grey dotted lines in Figure  
274 4B), confirming that the emergence of hubs is a direct fingerprint of the existence of well distinct  
275 substates.

276

277 Figure 4A also shows that some computing hubs are shared by different substates, while others  
278 are specific to one substate/one feature. In order to assess how substate-specific the computing  
279 hubs are, we use a measure of *similarity* (see Methods). A null value indicates that every substate  
280 has a unique hub set with no overlap between substates while a 1 value means that all substates  
281 have an identical distribution. Figure 4C shows that, in control animals, a majority of hubs tend  
282 to be substate-specific (similarity < 0.5). In CA1, the distribution of hubs is less substate-specific  
283 than in the mEC (higher similarity). In epilepsy, the distribution of hubs does not change in CA1,  
284 while hubs become significantly more substate-specific in the mEC. In other words, the status of  
285 being hub is for a mEC neuron less stable in epilepsy than in control animals.

286

287 We conclude that, in epilepsy, the mEC and CA1 display an increase in the number of neurons  
288 labeled as hubs at least once, and that the substate-specificity of hubs is increased in the mEC.  
289 Taken together, these two findings suggest a more hectic and random-like emergence of  
290 computing hubs in epilepsy as compared to control, albeit expressed in different ways; in mEC  
291 there are more hubs that are simultaneously more specific than control and in CA1 there are  
292 more hubs while staying the same, indicating a possible ‘shuffling’ of hubs. We believe this also  
293 further confirms that alterations in information processing are brain-region dependent.



294

295 **Figure 4 – Computing Hubs and their distributions –** (A) Example of computing hubs in the

296 control mEC extracted from a given state table. The y axis is unsorted neuron label, and the x axis

297 shows the substates for firing (5), storage (4) and sharing (6) features. A yellow bar indicates that

298 the given neuron is a computational hub during a substate. On the right is a summed version of

299 the graph on the left, visually showing the fraction of neurons that are a hub at least once (40%).

300 (B) The percentage of neurons that are hubs at least once is increased in epilepsy independently

301 of  $k_{tot}$ . The grey dotted line represents the mean of the shuffled, null model. (C) The similarity  
302 index plotted as a function of  $k_{tot}$ . The hubs become less substate-specific in the mEC in epilepsy.  
303 Blue and red are for control and epilepsy data, respectively. The bold lines are the mean, and the  
304 shaded regions are the 99% bootstrapped confidence interval.  
305

## 306 **Alterations in the core-periphery organization of CA1 computing hubs in epilepsy**

307 The partners from whom a given neuron receives or to whom it sends information are  
308 continuously changing (Clawson et al., 2019). At each time step, the instantaneous sharing  
309 networks can be seen as having a dynamic core-periphery structure (Pedreschi et al., 2020), with  
310 a core of tightly integrated neurons, surrounded by lightly connected periphery neurons. Two  
311 key measures of the core-periphery structure are the coreness, how central or well-integrated  
312 within a dense subnetwork – how “core”– a given neuron is, and the Jaccard index, a measure  
313 indicating how similar (or, conversely, liquid) the connections are between the recorded neurons  
314 between two time steps. We find that average coreness and the overall coreness distribution  
315 shapes are not significantly changed in epilepsy for either mEC or CA1 (Fig S5). Thus, the core-  
316 periphery architecture of information sharing networks within every substate is preserved in  
317 epilepsy. However, during the SO state, the average Jaccard values in CA1 are significantly  
318 decreased in epilepsy as compared to control (Fig S5). Thus, in CA1 there is enhanced connectivity  
319 variance and more volatile recruitment of neurons in the core.

320

## 321 **Assessing substate sequences**

322 The analysis of individual features (firing, storage and sharing) revealed brain state- and brain  
323 region-dependent alterations in epilepsy. We now focus on a more integrated view of the  
324 informational patterns, in which we consider both the simultaneity of the ongoing types of  
325 patterns and their articulation in sequences along time. We perform this higher-level exploration  
326 using the notion of information processing states (IPS), driven by the idea of symbolization, as  
327 shown in Figure 2A (Porta et al., 2015). From each analysis time window, we generate a four-

328 letter word, with the letters representing the substate labels of the global state, firing, storage  
329 and sharing features measured in this time window (see Methods). When the analysis window is  
330 shifted by 1 s, another word is obtained, which is identical to the previous one if the substate  
331 does not change. This procedure allows us to reduce the description of the complex simultaneous  
332 variations of firing, storage and sharing patterns within the neuronal population to simple strings  
333 of symbolic *words*, a sort of “neuronal language” built of sequences of possible words in a  
334 dictionary. We can then assess how the properties of these strings are modified in epilepsy at the  
335 level of their dictionary and syntax.

336

337 We defined all possible state tables generated through our k-means procedure as a *library* (Fig  
338 2). Now, as tables are considered as a sequence of words, we define the sequence of words  
339 generated as a *book*. The number of letters, and therefore the number of words, depend upon  
340  $k_{tot}$ . As a result, we label our differently generated books by  $k_{tot}$ . All 512 possible books per  
341 recording are grouped together to form a *library*. For each library, we build two sister libraries  
342 for comparison: one in which we sort every book internally to be highly ordered, and one in which  
343 we randomize every book internally to be highly disordered (see Methods). Using this word/book  
344 analogy, we begin to explore the organization of the language of the information processing  
345 contained in the books held within the library – What words are expressed? Is there a syntax, or  
346 organizational rules? And how does epilepsy change these measures?

347

348 **Impoverishment of the Dictionary in the mEC in Epilepsy**

349 For each  $k_{tot}$ , there is a fixed number of potential words that can be generated and possibly  
350 appear within the associated book (see cartoon in Figure 5A). As in any language, only a fraction  
351 of all possible words is expressed. For each book, we measure the used dictionary fraction, or  
352 *relative dictionary* (see Methods). Figure 5A illustrates two end cases. The low relative dictionary  
353 (left) uses a small number of expressed words, while the high relative dictionary (right) uses a  
354 much richer vocabulary, wherein almost all of the potential dictionary is expressed. While the  
355 measure of relative dictionary in and of itself is informative, it is difficult to use such a measure  
356 to assess meaningful changes (i.e., before control and epilepsy) without having comparative  
357 baselines. Therefore, we compute not only the relative dictionary of our libraries, but also that  
358 of the ordered and random sister libraries (which correspond to the null hypotheses of order and  
359 disorder in the ‘language’ of the book, respectively). We then apply a linear transformation to  
360 the relative dictionary measure, resulting in 0 representing the relative dictionary measure of  
361 ordered books, and a value of 1 representing a relative dictionary measure identical to that of  
362 randomized books. Such a normalized relative dictionary measure tracks not only the richness of  
363 the used dictionary but also its position between order and disorder.

364

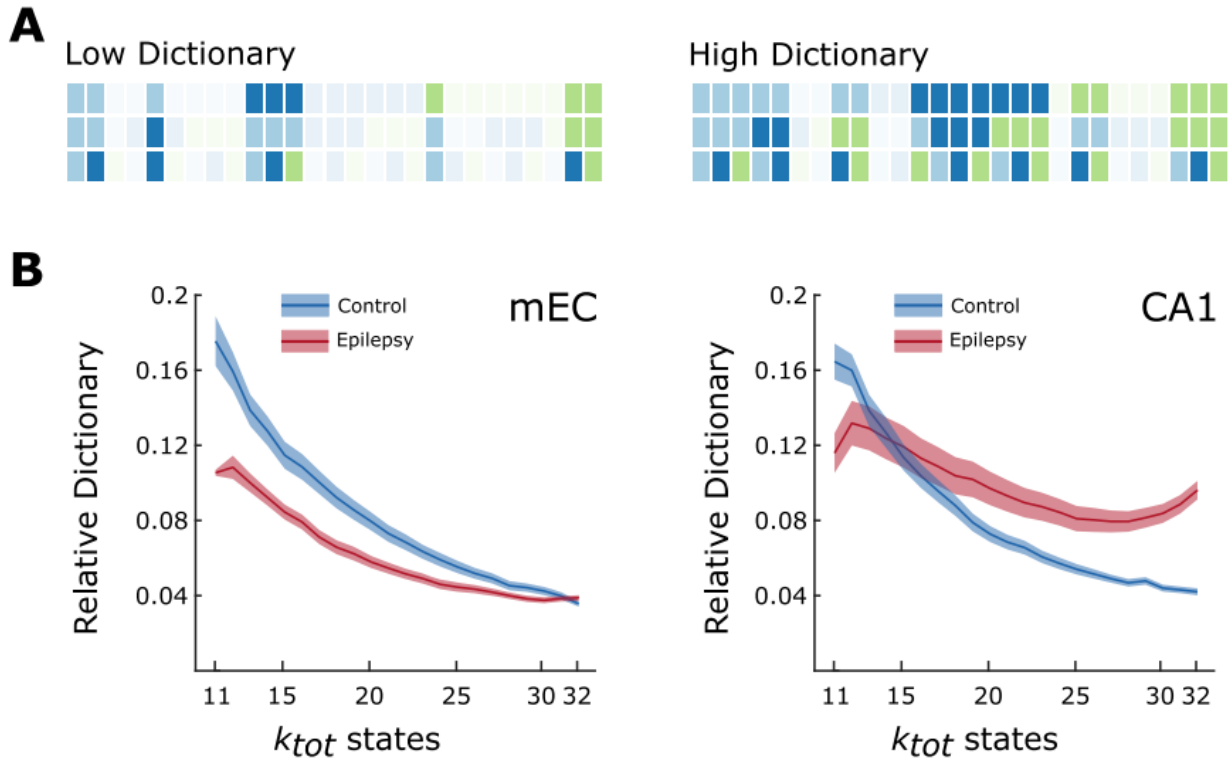
365 Figure 5B shows that for both the mEC and CA1 in control and epilepsy conditions, the normalized  
366 relative dictionaries lie much closer to 0 than to 1, meaning that their relative dictionaries are  
367 much more similar to a system with organization that is ordered than disordered. In epilepsy, the  
368 relative dictionary is reduced with respect to control in the mEC (Figure 5B). Thus, the dictionary  
369 of state dynamics language seems impoverished in the mEC in epilepsy. There is also a reduction

370 in CA1, but only for books with low  $k_{tot}$  values whereas it is increased for  $k_{tot} > 15$ . This 'crossing'  
371 of control and epileptic near  $k_{tot} = 15$  may be potentially explained by the strength of clustering for sharing  
372 features (Fig S3). Contrary to all features, there exists only a small window of  $k$  for sharing in CA1 in which  
373 k\_means clusters the feature better than a null model. Therefore, dictionaries made with poor clustering  
374 may drive the dictionary too high for low values of  $k$ . This is the first instance for which the generic  
375 rule that results should be independent of the choice of  $k$ , fails. However, this characterization  
376 of dictionaries further demonstrates that the alterations are brain region dependent.

377

378 The relative dictionary provides important information about the words, but not how words are  
379 organized in time. This is similar to the grammar, or syntax, of a traditional sentence. To analyze  
380 this syntax (how words are organized from one window not the next), we quantify the level of  
381 organization present in the state tables as a whole, i.e., the overall dynamics of a system moving  
382 though IPSs (Figure 2A).





383

384 **Figure 5 – Relative dictionaries within the libraries –** (A) Fictional cartoons representing two  
385 extremes for the measure of relative dictionary. Each row represents a feature (firing, storage,  
386 sharing); for simplicity we do not take into account the brain states (THE and SO). We consider  
387 three substates (light blue, dark blue, green) per feature (using the same color code for  
388 simplicity), which makes a total of  $3^3 = 27$  words (the representation is similar to counting in  
389 base 3 with color, increasing from left to right). Words that are not observed are shaded. A low  
390 relative dictionary (left) contains a low fraction of all possible words, while a high relative  
391 dictionary (right) contains a high fraction. (B) Relative dictionary values as a function of  $k_{tot}$ . As  
392 expected, the fraction of words used in control decreases as the number of possible words  
393 increases. The relative dictionaries are similar in mEC and CA1 in controls. There is a marked  
394 decrease in the relative dictionary in the mEC in epilepsy. In CA1, the relative dictionary in  
395 increased or decreased as compared to control as a function of  $k_{tot}$ . Blue is representative of

396 control data and red is representative of epileptic data. The bold lines are the mean, and the  
397 shaded regions are the 99% bootstrapped confidence interval.

398

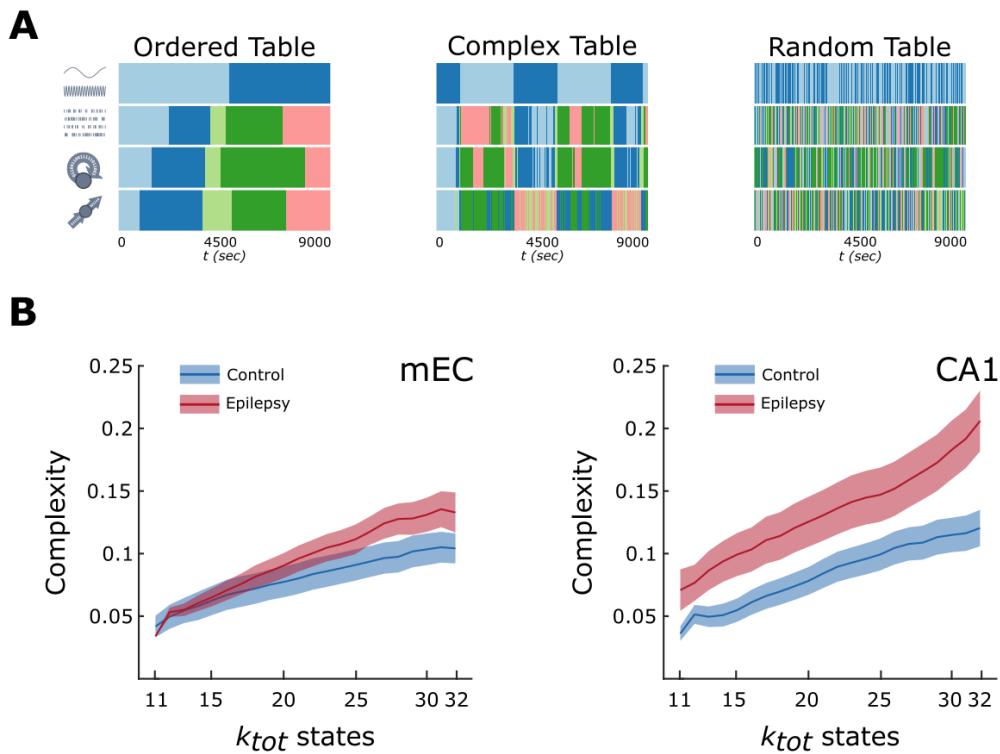
399 **The syntax of substate sequences is less regular in epilepsy**

400 Compressibility is a key property of an object as it represents the degree of internal order of the  
401 object. This is because any regularity within may be described by simply referencing its previous  
402 occurrence. Again, our state tables are bordered by two extreme cases: order and randomness  
403 (Figure 6A). An ordered table is dominated by a highly structured syntax, typically dominated by  
404 a lower dictionary and long periods of sustained words. Therefore, an ordered table is very  
405 compressible due to this internal order. A random table, on the other hand, typically contains an  
406 exceedingly high number of words, which follow each other in a disorderly (random) manner.  
407 This results in non-compressibility. A complex table is one that lies between those extremes. In  
408 order to characterize the complexity of the state tables, we compute a tailored form of  
409 description length complexity (Clawson et al., 2019; Rissanen, 1978), which is scaled to the sister  
410 libraries of order and disorder. Thus, in Figure 6B, 0 represents the complexity of the ordered  
411 library, something very compressible, while 1 represents the complexity of our disordered library,  
412 something very uncompressible (as shown in Figure 6A). In controls, the complexity is similar in  
413 mEC and CA1, close to an ordered table. In epilepsy, the complexity is significantly increased for  
414 all  $k_{tot}$  values, while it is increased in the mEC at the high end of our library.

415

416 Combining the results from Figures 5 & 6, we can propose the following interpretation. In CA1,  
417 the increase in complexity found in epilepsy, at least for books with sufficiently large  $k_{tot}$ , can be

418 explained, at least in part, by an enriched dictionary, since enrichment of the relative dictionary  
419 positively correlate with complexity (Clawson et al., 2019). In the mEC, the relative dictionary  
420 decreases while the complexity mildly increases. Thus, mEC books have a less regular syntax  
421 despite being constructed out of a lesser number of words.



422  
423 **Figure 6 – Order, disorder, and complexity** – (A) Examples of state tables, similar to that of Fig  
424 2A, from the mEC showing the two extremes of order and disorder as well as one of the possible  
425 state tables taken from the state table library. (B) Complexity values for both the mEC and CA1  
426 as a function of  $k_{tot}$ . The complexity is similar in mEC and CA1 in controls. In epilepsy, the  
427 complexity is largely increased in CA1, and only for large  $k_{tot}$  values for mEC. Blue is representative  
428 of control data and red is representative of epileptic data. The bold lines are the mean, and the  
429 shaded regions are the 99% bootstrapped confidence interval.

## 430 Discussion

431 This study provides evidence that epileptic conditions alter information processing in its simplest  
432 sense, the primitive storage and sharing operations as we introduce here, in a brain-region  
433 dependent manner. As these basic processes are necessarily involved in a variety of neural  
434 computations, their alterations may indirectly impact numerous cognitive functions.

435

436 The main limitation to our study is that it is made under anesthesia, versus for example, goal-  
437 directed behavior to assess cognitive function. The type of analysis we performed is powerful as  
438 it allows unraveling basic properties of information processing without needing to know which  
439 computations are ongoing. However, it requires long-duration, stable recordings with large state  
440 sampling to obtain enough data points to perform reliable statistics. We did not record during  
441 natural sleep, because seizures and interictal spikes (which would act as strong confounding  
442 factors) mostly occur during the light phase, while they do not occur under anesthesia. However,  
443 a similar type of analysis performed in control animals led to similar results during sleep and  
444 anesthesia (Clawson et al., 2019), suggesting that the anesthesia procedure we use does not  
445 significantly alter core information dynamics.

446

447 We refer to the elementary information storage and sharing operations as primitive (or low level)  
448 information processing operations, as we consider them as fundamental building blocks within  
449 an algorithm to reach an end condition (like a function), similar to the “algorithmic level”,  
450 introduced by Marr & Poggio (1977). Algorithm is used here in its most generic meaning, as we  
451 do not claim that the brain is analogous to a computer. Such primitive processing operations, as

452 we define them, represent nothing else than the emergent “informational effect” of very  
453 concrete neurophysiological phenomena. Storage and sharing of information directly derive from  
454 auto- and cross-correlations in firing, which widely vary in neuronal populations (Schneidman et  
455 al., 2006), and can be directly measured from spiking activity of neurons. Other primitive  
456 processing operations exist, such as information transfer (Palmigiano et al., 2017; Schreiber,  
457 2000) or information modification (Lizier et al., 2013; Wibral et al., 2017). Our recordings and  
458 choice of a time-resolved approach do not provide enough data to track these more sophisticated  
459 operations. However, the processing functions of storage and sharing are especially important as  
460 they represent statistical measures of information flow in time, and spacetime, respectively.

461

462 We show that primitive information processes are organized in temporal sequences of  
463 information processing substates (IPs), which are extracted via a cluster analysis. We have used  
464 a non-biased approach, spanning many possible combinations of numbers of clusters. The fact  
465 that most results are independent from the choice of the number of clusters provides a strong  
466 argument for the genericity of our conclusions. With this approach, we demonstrate a  
467 degradation of complexity due to enhanced randomness in epilepsy. This conclusion stems from  
468 the convergence of complementary analyses. First, storage and sharing hubs are less robust,  
469 waxing and waning in a more erratic manner across substates and the recruitment of neurons  
470 into the integrated core of sharing networks is more volatile. Second, average storage and  
471 sharing strength are more similar between brain states, and this “dedifferentiation” occurs  
472 despite the higher contrast between substates. Third, the state specificity of IPS is reduced, i.e.,  
473 many IPs are now redundant between THE or SO. Together, these results imply that a change in

474 brain state is no longer associated to strong specificity in information processing. Fourth, freed  
475 from the constraint of being strongly state-specific, the relative dictionary in epilepsy could, in  
476 principle, be increased. However, mEC has a decreased relative dictionary, which instead implies  
477 an ability to form unique IPSs. Yet, the description complexity of IPS sequences tends to be larger  
478 in epilepsy than control. In other words, IPS sequences have a less regular syntax despite being  
479 assembled out of less unique words.

480

481 The IPS dynamics of CA1 show, in general, less alterations than that of mEC. The fact that  
482 information processing is affected in brain region-dependent manner is an important result. The  
483 mEC and CA1 have distinct cytoarchitectures and different fates following an epileptogenic insult.  
484 Most striking is the loss of layer 3 in the mEC, and the injury of many pyramidal cells and  
485 interneurons in the CA1 region (Curia et al., 2008). It is not possible to assign a given alteration  
486 in information processing to a given morpho-functional changes in the mEC or CA1. Global brains  
487 states (THE and SO) and IPSs are emergent properties. Any change in any brain region can  
488 potentially affect neuronal dynamics anywhere from the local to the global scale. Therefore, the  
489 morpho-functional alterations in mEC or CA1 may contribute to any combination of local and  
490 global changes. However, changes in terms of information processing do not necessarily have to  
491 be homogenous across brain regions. In fact, brain region-specific modifications are expected as  
492 each region is embedded in different functional networks. How these brain-region specific  
493 changes contribute to comorbidities (such as cognitive deficit, anxiety, and depression) remain  
494 to be determined.

495

496 Our measure of complexity is that of compressibility, accounting for the internal structure, i.e.,  
497 how internally ordered are IPS syntaxes. Any change in this internal organization would thus  
498 imply an underlying change in algorithmic operation, resulting in different computation in control  
499 and epilepsy conditions. Our measure of complexity does not allow distinguishing between an  
500 increase in processing versus an increase in noise, as complexity would grow in both cases. Other  
501 measures can be used, but they would require more data (Crutchfield, 2011). However, in CA1,  
502 books with large  $k_{tot}$  have an increased, rather than decreased dictionary size, which may explain  
503 the strong increase in sequence complexity. It is not clear, however, that this dictionary increase  
504 is a positive factor as it may reflect a more irregular IPS selection, with rare IPSs indicating  
505 dysfunction in IPS sequential production. Another possibility is that boosted IPS sequence  
506 complexity in CA1 and, at a lesser extent, mEC is a compensatory mechanism to generate a more  
507 sophisticated syntax to compensate for other shortages, such as reduced hub stability and  
508 degraded state-specificity of IPS.

509  
510 In a biological context, the algorithmic level change comes as a result of altered collective, spiking  
511 activity and could lead to an entirely different expression of higher-level behavior, such as  
512 cognition. However, the question of whether this increase of complexity (decrease of internal  
513 order) observed in epilepsy is the source of cognitive deficits or not remains ultimately open. It  
514 has been theorized that “biological systems manipulate spatial and temporal structure to  
515 produce order – low variance – at local scales” in an effort to adapt and survive (Flack, 2019).  
516 Therefore, if networks are still functional in epilepsy conditions, are these manipulations now  
517 less effective? Or is the resulting low variance order now too difficult to sustain due to a

518 combination of physiological and functional changes? These issues remain to be addressed.  
519 Nevertheless, the approaches presented here introduce valuable insight into aspects of the  
520 collective behavior of neural populations, and provide a quantitative framework to answer such  
521 questions.

522

523 In conclusion, the framework we introduce here to compare information processing between  
524 control and epilepsy, can be generalized to neurological disorders. Since most, if not all, of the  
525 latter, including migraine, Alzheimer's disease, and Parkinson's disease are associated with co-  
526 morbidities, it will be particularly interesting to determine whether information processing at the  
527 algorithmic level is also affected in these disorders. Following the principle of degeneracy (Prinz  
528 et al., 2004), very different structural alterations, which characterize different neurological  
529 disorders, may produce similar alterations in information processing, providing an explanation  
530 for the commonalities of co-morbidities across different disorders.

531

## 532 **Methods**

### 533 **Ethics**

534 All experiments were conducted in accordance with Aix-Marseille Université and Inserm  
535 Institutional Animal Care and Use Committee guidelines. The protocol was approved by the  
536 French Ministry of National Education, Superior Teaching, and Research, under the authorization  
537 number 01451-02. All surgical procedures were performed under anesthesia and every effort  
538 was made to minimize suffering and maximize the animals' wellbeing from their arrival to their  
539 death. All the animals were housed in pairs in large cages with minimal enrichment, food and



540 water at libitum, in a room with controlled environment (temperature:  $22 \pm 1$  °C; 12 h light/dark  
541 schedule with lights off at 8:00 pm; hygrometry: 55%; ventilation: 15-20 vol/h).

542 **Data information.**

543 We use in this work a portion of the data (5 out of 7 original experiments) initially published by  
544 Clawson et al. 2019 as control data, which includes local field potentials (LFPs) and single-unit  
545 recordings obtained from the dorsomedial entorhinal cortex (mEC) and the dorsal hippocampus  
546 (HPC) of anesthetized rats. Six recordings are original data, which includes LFPs and single-units  
547 recorded in the mEC and HPC recorded simultaneously under anesthesia in epileptic condition.  
548 See Figures S1 for details on recordings, number of cells, and layers recorded.

549 **Epilepsy model and surgery.**

550 We induced status epilepticus (SE) on 6 male Wistar (250–400 g; Charles Rivers) by a single  
551 intraperitoneal (IP) injection of pilocarpine (320 mg/kg; Sigma-Aldrich), one week after receiving  
552 the animals from the vendor. To reduce peripheral effects, rats were pre-treated with methyl-  
553 scopolamine (1 mg/kg, IP; Sigma-Aldrich) 30 min before the pilocarpine injection. SE was stopped  
554 by diazepam (10 mg/kg, IP, two doses within a 15-min interval) after 60 min. Then the animals  
555 were hydrated with saline (2 ml, IP, twice within 2 h) and fed with a porridge made of soaked  
556 pellets, until they resumed normal feeding behavior.

557 At least 8 weeks after SE induction, we performed acute recordings. Rats were first quickly placed  
558 in isoflurane (4% in 2l/min O<sub>2</sub>) and injected IP with urethane (1.5 g/kg) and ketamine/xylazine (20  
559 and 2 mg/kg, IM), additional doses of ketamine/xylazine (2 and 0.2 mg/kg) being supplemented  
560 during the electrophysiological recordings. At all times the body temperature was monitored and  
561 kept constant with a heating pad. Heart rate, breathing rate, pulse distension, and arterial oxygen

562 saturation were also monitored with an oximeter (MouseOX; StarrLife Sciences) during the  
563 duration of the experiment to ensure the stability of the anesthesia and monitor the vital  
564 constants. The head was fixed in a stereotaxic frame (Kopf) and the skull was exposed and  
565 cleaned. Two miniature stainless-steel screws driven into the skull above the cerebellum served  
566 as ground and reference electrodes. Two craniotomies were performed to reach the mEC and  
567 the CA1 field of the HPC, respectively: from bregma: -7.0 mm AP and +4.0 mm ML; and from  
568 bregma: -3.0 mm AP and +2.5 mm ML. We chose these coordinates to respect known anatomical  
569 and functional connectivity in the cortico-hippocampal circuitry (Witter et al., 1988; Witter et al.,  
570 1989). Two 32-site silicon probes (NeuroNexus) were mounted on a stereotaxic arm each. A  
571 H1x32-10mm-50-177 was lowered at 5.0-5.2 mm from the brain surface with a 20° angle to reach  
572 the dorso-medial portion of the mEC, and a H4x8-5mm-50-200-177 probe was lowered at 2.5  
573 mm from the brain surface with a 20° angle to reach dorsal CA1. The on-line positioning of the  
574 probes was assisted by: the presence of unit activity in cell body layers and the reversal of theta  
575 ([3 6] Hz in anesthesia) oscillations when passing from layer 2 to 1 for the mEC probe, and the  
576 presence in *stratum pyramidale* either of unit activity and ripples (80-150 Hz) for the HPC probe.  
577 At the end of the recording, the animals were injected with a lethal dose of Pentobarbital Na  
578 (150mk/kg, i.p.) and perfused intracardially with 4% paraformaldehyde solution. We confirmed  
579 the position of the electrodes (DiIC18(3) (catalog #46804A, InterChim) was applied on the back  
580 of the probe before insertion) histologically on 40 µm Nissl-stained section as reported previously  
581 in detail (Ferraris et al., 2018; Quilichini et al., 2010). We used only experiments with appropriate  
582 position of the probe for analysis.

583 **Data collection and spike sorting.**

584 Extracellular signal recorded from the silicon probes was amplified (1000x), bandpass filtered (1  
585 Hz to 5 kHz) and acquired continuously at 32 kHz with a 64-channel DigitalLynx (Neuralynx) at  
586 16-bit resolution. We preprocessed the raw data using a custom-developed suite of programs  
587 (Csicsvari et al., 1999). The signals were down-sampled to 1250 Hz for the local field potential  
588 (LFP) analysis. Spike sorting was performed automatically, using KLUSTAKWIK  
589 (<http://klustakwik.sourceforge.net> (Harris et al., 2000)), followed by manual adjustment of the  
590 clusters, with the help of auto-correlogram, cross-correlogram and spike waveform similarity  
591 matrix (KLUSTERS software package, <http://klusters.sourceforge.net> (Hazan et al., 2006)). After  
592 spike sorting, we plotted the spike features of units as a function of time, and we discarded the  
593 units with signs of significant drift over the period of recording. Moreover, only units with clear  
594 refractory periods and well-defined cluster were included in the analyses (Harris et al., 2000).  
595 Recording sessions were divided into brain states of theta (THE) and slow oscillation (SO) periods  
596 using a visual selection from the ratios of the whitened power in the HPC LFP [3 6] Hz theta band  
597 and the power of the mEC LFP neighboring bands ([1 3] Hz and [7 14] Hz), and assisted by visual  
598 inspection of the raw traces (Ferraris et al., 2018; Quilichini et al., 2010). We then used band-  
599 averaged powers over the same frequency ranges of interest as features for the automated  
600 extraction of spectral states via unsupervised clustering, which confirmed our manual  
601 classification. We determined the layer assignment of the neurons from the approximate location  
602 of their soma relative to the recording sites (with the largest- amplitude unit corresponding to  
603 the putative location of the soma), the known distances between the recording sites, and the  
604 histological reconstruction of the recording electrode tracks. Animals were recorded for at least  
605 two hours in order to get few alternations of THE and SO episodes.

## 606 **Feature Computation**

607 As in our previous work, for each region recorded we computed 4 main features from the  
608 electrophysiological data: global oscillatory band, neuronal firing sets, active information storage  
609 and the information sharing. We also keep the same sliding window paradigm where each  
610 feature is computed within a *10 second* window, and then the window is then moved forward in  
611 time *1 second*, which gives a *9 second* overlap. Therefore, when features are computed as  
612 described below, they are computed in this windowed fashion. The global oscillatory band  
613 features were computed by examining the LFP from both EC and CA1 and computing spectral  
614 power within 8 unequally sized frequency ranges (0–1.5 Hz, 1.5–2 Hz, 2–3 Hz, 3–5 Hz, 5–7 Hz, 7–  
615 10 Hz, 10–23 Hz and 23–50 Hz), averaged over all channels within each of the recorded layers.

616 Firing sets, active information storage, and the information sharing networks were all computed  
617 using a binarized raster built from the temporal labeling of spike firing (see Data Collection and  
618 Spike Sorting). Spiking data was binned using a *50 ms* bin; if a neuron fired within a given bin the  
619 output is a '1', and if not, a '0'. This, for example would mean that a 2-hour recording would be  
620 transformed from a *7200 second*  $\times$  *N* neuron matrix to a *7200000*  $\times$  *N* neuron matrix that is  
621 composed solely of 0's and 1's. Firing sets were computed by computing the average firing  
622 density for each neuron within a window, and after these averages were compiled into time-  
623 dependent vectors. This resulting matrix is the *Firing Features*. Active information storage was  
624 computed by measuring the mutual information of a neuron's binarized spike train between a  
625 given window and the window previous. What active information storage seeks to capture is the  
626 temporal ordering of individual spiking neurons, rather than capturing neurons that fire  
627 temporally close to one another (such as in the firing features). The resulting matrix is the *Storage*

628 *Features*. Information sharing is computed by measuring the mutual information between a given  
629 neuron's binarized spike train within a window and another neuron's binarized spike train in the  
630 window previous. This process is iterated over all possible neuron pairs. Information sharing  
631 captures a similar metric to that of active information storage, although the key difference is that  
632 information sharing captures not just the temporal ordering, but the spatio-temporal ordering of  
633 spike timing, as it is computed across neuron pairs, rather than individual neurons. The resulting  
634 matrix is the *Information Sharing*. Although these measures have only been briefly described  
635 here, we suggest to the interested reader to examine the methods presented in our previous  
636 work [REF] where they have been rigorously defined.

637

### 638 **Feature-Based Substate Extraction**

639 State extraction for each recording were also computed using the methods of our previous work,  
640 namely based around k-means clustering of each feature. The exception here, is we no longer  
641 choose a stable number of K clusters in k-means. Rather we cluster our 3 raster-based computed  
642 features (firing, storage, sharing) 3 separate times with K ranging from K = 3, 4, ... 10. The function  
643 'kmeans' was used from the default MATLAB toolbox. More information can be found on the  
644 Mathworks website. These K values were chosen as they represented a clustering range of too  
645 gross to too fine based on previous findings.  $K \leq 2$  would represent the same, or less, number  
646 of states as global states, which was previously established to be too small (Clawson et al., 2019).  
647 The clustering became too fine when  $K \geq 10$ , wherein many substates only appeared for brief  
648 time periods, and never re-occurred. For each feature there are 8 different clustering results,  
649 done in an unsupervised manner 3 times to ensure that our results do not rely on single instance

650 of clustering. This gave our analysis an opportunity to compute all metrics defined below over a  
651 robust range of K, ensuring that we can investigate how our substate stable metrics and results  
652 vary with arbitrarily too little or too many substates.

653

654 To compute the null model for substate extraction the process detailed above was repeated with  
655 the time stamps of all firing, storage and sharing jittered. This therefore retains the global mean  
656 and variance. Then, k-means was run on this jittered dataset 3 times, to produce 3 different  
657 clustering of the randomized dataset. These were not modified after this step and were used in  
658 any instances where a null model was needed (i.e. for silhouette and contrast).

659

#### 660 **Substate Tables**

661 Our main meta-object of study is a state table, a combination of our four features into a matrix  
662 (4 x number of windows). Table generation is an iterative process, as we have 8 possible substate  
663 configurations per feature. First,  $k = 3$  in cluster attempt 1 for firing ( $FIRE_{k3C1}$ ),  $k = 3$  in cluster  
664 attempt 1 for storage ( $STORE_{k3C1}$ ), and  $k = 3$  in cluster attempt 1 for sharing ( $SHARE_{k3C1}$ ), are used  
665 in conjunction with the clustered spectral substates to form substate table 1 (Figure 2A).

666

667 Then,  $FIRE_{k3C1}$ ,  $STORE_{k3C1}$ , and  $SHARE_{k4C1}$  are used in conjunction with the clustered spectral  
668 substates to form substate table 2. After,  $FIRE_{k3C1}$ ,  $STORE_{k3C1}$ , and  $SHARE_{k5C1}$  used in conjunction  
669 with the clustered spectral substates to form substate table 3. This process continues such that  
670 all combinations of possible k values have been saved for a total of 512 different substate tables,  
671 with the final table having  $FIRE_{k10C1}$ ,  $STORE_{k10C1}$ , and  $SHARE_{k10C1}$ . It is important to note that all

672 tables have the same spectral clustering, as the 2 substates of SO and THE are extremely robust  
673 as discussed above. This entire process is then repeated for each clustering attempt, resulting in  
674 3 sets of our 512 substate tables for each region for each recording. Where applicable, all results  
675 are given as a function of total k states per table (i.e. for state table 1, there are 2 global states,  
676 3 firing, 3 storage and 3 sharing for a total  $k_{\text{total}} = 11$ ).

677

678 To produce the ordered tables for the ‘ordered’ null model, each substate table was sorted such  
679 that all substates with label ‘1’ appeared first, label ‘2’ was second, and so on and so forth. This  
680 can easily be achieved with the MATLAB function *sort*. Note that there is only one possible  
681 version of this type of ordering, and therefore the sample size for ordered tables is the same as  
682 recordings ( $n = 5$  for control,  $n = 6$  for epilepsy). To produce the randomized tables, substate  
683 labels were randomly permuted in time. For this process, we used bootstrapping to produce as  
684 5000 randomizations to ensure the random null model was as strong as possible. To do this, 90%  
685 of each table was taken, randomly permuted and saved. These resulting tables were used as the  
686 random null model for relative dictionary and complexity seen in Figure 5 & 6.

687

## 688 **Contrast**

689 To calculate contrast for a given feature we first calculate its global mean for each neuron (i.e.,  
690 global mean firing per neuron). Here, ‘global’ refers to the entire recording. We then calculate  
691 the substate mean for each neuron by concatenating all periods of a given substate and  
692 calculating the mean across the ‘entire’ substate. The formula for contrast is then defined as the

693 difference between the substate mean firing rate and the global mean firing rate, normalized by  
694 the global mean firing rate.

$$695 \quad \text{contrast} = \frac{\mu_{\text{substate}} - \mu_{\text{global}}}{\mu_{\text{global}}}$$

696 This allows the contrast to be either positive or negative. This process was done for all 3 features  
697 of firing, storage and sharing such that there are contrast values for each. This process was  
698 repeated for all possible clustering, therefore a contrast value per feature per  $k$ .

699

### 700 **Substate-Specificity**

701 To compute the distribution of substates within periods of SO and THE we counted the number  
702 of times a substate appeared within a given epoch. Some substates exclusively appeared in only  
703 SO or THE, while others occurred in both. From these frequencies we estimated  $p(\text{THE})$  and  
704  $p(\text{SO})$ , i.e. the probability of a given substate occurring in either THE or SO, respectively. SSI is  
705 then:

$$706 \quad \text{SSI} = |p(\text{THE}) - p(\text{SO})|$$

707 This equation results in SSI bound between 0 and 1, where 1 represents a state who exclusively  
708 occurs in either THE or SO and 0 represents a state that occurs equally in THE and SO.

709

### 710 **Hubs & Hub Stability**

711 In this work we define a hub neuron in the same way as our previous work. Namely, for a given  
712 feature if a neuron's activity within a given substate was higher than the 90<sup>th</sup> percentile it was  
713 marked as a hub for the feature for that state. We compute hubs for every iteration of state table  
714 as defined above, such that we have a graph, or matrix, (see FIG 4A) for each state table. These



715 matrices are  $\text{Neuron} \times k_{\text{total}}$  where each entry is either a '0' for non-hub or '1' for hub. To compute  
716 how stable each of these matrices are as a function of  $k$ , we compute the normalized hamming  
717 distance of each matrix using the *pdist2* function in MATLAB but modified so that it gives a sense  
718 of how stable hubs are across states, where perfect similarity would result in a '1', and no  
719 similarity at all would give a '0'.

720

### 721 **Coreness & Jaccard**

722 The values for coreness & Jaccard were computed using the methods presented in Pedreschi et  
723 al. (2020). These were then analyzed using the same sliding window technique as presented in  
724 'Feature Computation'. After, periods of THE and SO were analyzed with similar techniques as  
725 that of Figure 1.

726

### 727 **Dictionary & Complexity**

728 To compare sequences of substates of different types or in different regions we introduced a  
729 symbolic description of substate switching. With this description, each substate label acts as a  
730 letter symbol  $s^{(p)}$ , where  $(p)$  can indicate firing, sharing or storage. For example, the firing features  
731 from the example substate table 1 [FIG 2A] would have the integer labels 1, 2, 3, and 4 (they can  
732 also arbitrarily be assigned letters as well, i.e. A, B, and C). We can therefore describe the  
733 temporal sequences of the visited substates of each feature as an ordered list of integers  $s^{(p)}(t)$ .  
734 Once substate labels are thought of as letters, we define the combination of firing, storage and  
735 sharing letters in each state table from a given window as 3 letter *words*. Using the formalism of  
736 linguistics, we can then compute the *dictionary*, or the number of words expressed, of a given

737 recording within a region. We can also compute the *used dictionary fraction*, or the number of  
738 words found in the dictionary divided by the number of theoretically possible words given the  
739 number of substates per feature. For example, substate table 1 could have expressed 27 unique  
740 words. The used dictionary fraction was computed in an identical way to that of Clawson et al  
741 2019. Specially, see ‘Complexity of substates sequences.

742

743 Using these methods, we compute the complexity of the sequences expressed using the notions  
744 of Kolmogorov-Chaitin complexity and minimum description length approaches (Crutchfield,  
745 2011). While further discussion of method can be found here (Clawson et al., 2019) – the aspects  
746 of this complexity measure that is relevant for this work is that a random sequence of letters (and  
747 words) produces a higher complexity, while an ordered sequence of letters (and words) would  
748 produce a low complexity.

749

## 750 **Ordered & Random Substate Tables**

751 To have relevant points of reference in our measures, each substate table was ordered and  
752 randomized. For the case of ordering, all substate labels for all features were sorted in ascending  
753 order which keeps the total lifetime of any state constant, while removing the temporal  
754 organization in an *ordered* fashion. In the case of randomization, all substate labels for all features  
755 were randomized 500 times, which again keeps the total lifetime of any state constant, while  
756 removing the temporal organization in a *random* fashion.

757 To compute the relative minimums and maximums for comparisons between order and random  
758 the MATLAB function ‘rescale’ was used. The minimums were computed using the average (of a

759 given measure) of all ordered state tables for a given  $k_{\text{total}}$  and the maximums were computed  
760 using the average (of a given measure) of all random substate tables for a given  $k_{\text{total}}$ .

## 761 **Plotting**

762 Various tools were used for plotting. While mostly done via MATLAB, other tools were also  
763 used from 'Moving Beyond p-values' (Ho et al., 2019).

764

## 765 **Bibliography**

766 Barba, C., Barbati, G., Minotti, L., Hoffmann, D., & Kahane, P. (2007, Jul). Ictal clinical and scalp-EEG  
767 findings differentiating temporal lobe epilepsies from temporal 'plus' epilepsies. *Brain*, *130*(Pt  
768 7), 1957-1967. <https://doi.org/10.1093/brain/awm108>

769

770 Bartolomei, F., Chauvel, P., & Wendling, F. (2008, Jul). Epileptogenicity of brain structures in human  
771 temporal lobe epilepsy: a quantified study from intracerebral EEG. *Brain*, *131*(Pt 7), 1818-1830.  
772 <https://doi.org/10.1093/brain/awn111>

773

774 Blumcke, I., Thom, M., Aronica, E., Armstrong, D. D., Bartolomei, F., Bernasconi, A., Bernasconi, N., Bien,  
775 C. G., Cendes, F., Coras, R., Cross, J. H., Jacques, T. S., Kahane, P., Mathern, G. W., Miyata, H.,  
776 Moshe, S. L., Oz, B., Ozkara, C., Perucca, E., Sisodiya, S., Wiebe, S., & Spreafico, R. (2013, Jul).  
777 International consensus classification of hippocampal sclerosis in temporal lobe epilepsy: a Task  
778 Force report from the ILAE Commission on Diagnostic Methods. *Epilepsia*, *54*(7), 1315-1329.  
779 <https://doi.org/10.1111/epi.12220>

780

781 Calhoun, V. D., Miller, R., Pearlson, G., & Adali, T. (2014, Oct 22). The chronnectome: time-varying  
782 connectivity networks as the next frontier in fMRI data discovery. *Neuron*, *84*(2), 262-274.  
783 <https://doi.org/10.1016/j.neuron.2014.10.015>

784

785 Chauvière, L., Raftafi, N., Thinus-Blanc, C., Bartolomei, F., Esclapez, M., & Bernard, C. (2009). Early  
786 deficits in spatial memory and theta rhythm in experimental temporal lobe epilepsy. *Journal of*  
787 *Neuroscience*, *29*(17), 5402-5410. <https://doi.org/29/17/5402> [pii] 10.1523/JNEUROSCI.4699-  
788 08.2009

789

790 Clawson, W., Vicente, A. F., Ferraris, M., Bernard, C., Battaglia, D., & Quilichini, P. P. (2019, Jun).  
791 Computing hubs in the hippocampus and cortex. *Sci Adv*, *5*(6), eaax4843.  
792 <https://doi.org/10.1126/sciadv.aax4843>

793

- 794 Crutchfield, J. P. (2011). Between order and chaos. *Nature Physics*, 8(1), 17-24.  
795 <https://doi.org/10.1038/nphys2190>
- 796  
797 Csicsvari, J., Hirase, H., Czurko, A., Mamiya, A., & Buzsáki, G. (1999). Oscillatory coupling of hippocampal  
798 pyramidal cells and interneurons in the behaving Rat. *Journal of Neuroscience*, 19(1), 274-287.  
799 <https://doi.org/10.1523/JNEUROSCI.19-01-00274.1999>
- 800  
801 Curia, G., Longo, D., Biagini, G., Jones, R. S., & Avoli, M. (2008, Jul 30). The pilocarpine model of temporal  
802 lobe epilepsy. *J Neurosci Methods*, 172(2), 143-157.  
803 <https://doi.org/10.1016/j.jneumeth.2008.04.019>
- 804  
805 de Barros Lourenco, F. H., Marques, L. H. N., & de Araujo Filho, G. M. (2020, Jul). Electroencephalogram  
806 alterations associated with psychiatric disorders in temporal lobe epilepsy with mesial sclerosis:  
807 A systematic review. *Epilepsy Behav*, 108, 107100. <https://doi.org/10.1016/j.yebeh.2020.107100>
- 808  
809 Ferraris, M., Ghestem, A., Vicente, A. F., Nallet-Khosrofian, L., Bernard, C., & Quilichini, P. P. (2018, Mar  
810 21). The Nucleus Reuniens Controls Long-Range Hippocampo-Prefrontal Gamma  
811 Synchronization during Slow Oscillations. *J Neurosci*, 38(12), 3026-3038.  
812 <https://doi.org/10.1523/JNEUROSCI.3058-17.2018>
- 813  
814 Flack, J. C. (2019). *Life's Information Hierachy*. Sante Fe Institute Press.
- 815  
816 Harris, K. D., Henze, D. A., Csicsvari, J., Hirase, H., & Buzsáki, G. (2000). Accuracy of tetrode spike  
817 separation as determined by simultaneous intracellular and extracellular measurements. *Journal*  
818 *of Neurophysiology*, 84(1), 401-414.
- 819  
820 Hazan, L., Zugaro, M., & Buzsáki, G. (2006). Klusters, NeuroScope, NDManager: a free software suite for  
821 neurophysiological data processing and visualization. *J Neurosci Methods*, 155(2), 207-216.  
822 <https://doi.org/10.1016/j.jneumeth.2006.01.017>
- 823  
824 Hesdorffer, D. C. (2016, Jun). Comorbidity between neurological illness and psychiatric disorders. *CNS*  
825 *Spectr*, 21(3), 230-238. <https://doi.org/10.1017/S1092852915000929>
- 826  
827 Ho, J., Tumkaya, T., Aryal, S., Choi, H., & Claridge-Chang, A. (2019, Jul). Moving beyond P values: data  
828 analysis with estimation graphics. *Nat Methods*, 16(7), 565-566.  
829 <https://doi.org/10.1038/s41592-019-0470-3>
- 830  
831 Holmes, G. L. (2015, Jun). Cognitive impairment in epilepsy: the role of network abnormalities. *Epileptic*  
832 *Disord*, 17(2), 101-116. <https://doi.org/10.1684/epd.2015.0739>
- 833

- 834 Inostroza, M., Brotons-Mas, J. R., Laurent, F., Cid, E., & de la Prida, L. M. (2013, Nov 6). Specific  
835 impairment of "what-where-when" episodic-like memory in experimental models of temporal  
836 lobe epilepsy. *J Neurosci*, 33(45), 17749-17762. [https://doi.org/10.1523/JNEUROSCI.0957-](https://doi.org/10.1523/JNEUROSCI.0957-13.2013)  
837 [13.2013](https://doi.org/10.1523/JNEUROSCI.0957-13.2013)
- 838
- 839 Kirst, C., Timme, M., & Battaglia, D. (2016, Apr 12). Dynamic information routing in complex networks.  
840 *Nat Commun*, 7(7), 11061. <https://doi.org/10.1038/ncomms11061>
- 841
- 842 Krishnan, V. (2020, Jul 14). Depression and Anxiety in the Epilepsies: from Bench to Bedside. *Curr Neurol*  
843 *Neurosci Rep*, 20(9), 41. <https://doi.org/10.1007/s11910-020-01065-z>
- 844
- 845 Lenck-Santini, P. P., & Holmes, G. L. (2008, May 7). Altered phase precession and compression of  
846 temporal sequences by place cells in epileptic rats. *J Neurosci*, 28(19), 5053-5062.  
847 <https://doi.org/10.1523/JNEUROSCI.5024-07.2008>
- 848
- 849 Lenck-Santini, P. P., & Scott, R. C. (2015, Sep 3). Mechanisms Responsible for Cognitive Impairment in  
850 Epilepsy. *Cold Spring Harb Perspect Med*, 5(10). <https://doi.org/10.1101/cshperspect.a022772>
- 851
- 852 Lizier, J. T., Atay, F. M., & Jost, J. (2012, Aug). Information storage, loop motifs, and clustered structure in  
853 complex networks. *Phys Rev E Stat Nonlin Soft Matter Phys*, 86(2 Pt 2), 026110.  
854 <https://doi.org/10.1103/PhysRevE.86.026110>
- 855
- 856 Lizier, J. T., Flecker, B., & Williams, P. L. (2013). Towards a Synergy-based Approach to Measuring  
857 Information Modification. *2013 Ieee Symposium on Artificial Life (Alife)*, 43-51.  
858 <https://doi.org/10.1109/ALIFE.2013.6602430>
- 859
- 860 Lopez-Pigozzi, D., Laurent, F., Brotons-Mas, J. R., Valderrama, M., Valero, M., Fernandez-Lamo, I., Cid, E.,  
861 Gomez-Dominguez, D., Gal, B., & Menendez de la Prida, L. (2016, Nov-Dec). Altered Oscillatory  
862 Dynamics of CA1 Parvalbumin Basket Cells during Theta-Gamma Rhythmopathies of Temporal  
863 Lobe Epilepsy. *eNeuro*, 3(6). <https://doi.org/10.1523/ENEURO.0284-16.2016>
- 864
- 865 Marr, D. C., & Poggio, T. (1977). From Understanding Computation to Understanding Neural Circuitry.  
866 *Neurosciences Research Program Bulletin*, 15(3), 470-491. <Go to ISI>://WOS:A1977EH37300024
- 867
- 868 Palmigiano, A., Geisel, T., Wolf, F., & Battaglia, D. (2017, Jul). Flexible information routing by transient  
869 synchrony. *Nat Neurosci*, 20(7), 1014-1022. <https://doi.org/10.1038/nn.4569>
- 870
- 871 Pedreschi, N., Bernard, C., Clawson, W., Quilichini, P., Barrat, A., & Battaglia, D. (2020). Dynamic core-  
872 periphery structure of information sharing networks in entorhinal cortex and hippocampus.  
873 *Network Neuroscience*, 1-30. [https://doi.org/10.1162/netn\\_a\\_00142](https://doi.org/10.1162/netn_a_00142)
- 874

- 875 Porta, A., Baumert, M., Cysarz, D., & Wessel, N. (2015, Feb 13). Enhancing dynamical signatures of  
876 complex systems through symbolic computation. *Philos Trans A Math Phys Eng Sci*, 373(2034).  
877 <https://doi.org/10.1098/rsta.2014.0099>
- 878  
879 Prinz, A. A., Bucher, D., & Marder, E. (2004, Dec). Similar network activity from disparate circuit  
880 parameters. *Nat Neurosci*, 7(12), 1345-1352. <https://doi.org/10.1038/nn1352>
- 881  
882 Quilichini, P., Sirota, A., & Buzsáki, G. (2010). Intrinsic circuit organization and theta-gamma oscillation  
883 dynamics in the entorhinal cortex of the rat. *J Neurosci*, 30(33), 11128-11142.  
884 <https://doi.org/10.1523/JNEUROSCI.1327-10.2010>
- 885  
886 Quilichini, P. P., & Bernard, C. (2012). Brain state-dependent neuronal computation. *Front Comput*  
887 *Neurosci*, 6, 77. <https://doi.org/10.3389/fncom.2012.00077>
- 888  
889 Rissanen, J. (1978). Modeling by shortest data description. *Automatica*, 14(5), 465-471.  
890 [https://doi.org/10.1016/0005-1098\(78\)90005-5](https://doi.org/10.1016/0005-1098(78)90005-5)
- 891  
892 Rusina, E., Bernard, C., & Williamson, A. (2021). Kainic Acid Models of Temporal Lobe Epilepsy. *eNeuro*.
- 893  
894 Schneidman, E., Berry, M. J., 2nd, Segev, R., & Bialek, W. (2006, Apr 20). Weak pairwise correlations  
895 imply strongly correlated network states in a neural population. *Nature*, 440(7087), 1007-1012.  
896 <https://doi.org/10.1038/nature04701>
- 897  
898 Schreiber, T. (2000, Jul 10). Measuring information transfer. *Phys Rev Lett*, 85(2), 461-464.  
899 <https://doi.org/10.1103/PhysRevLett.85.461>
- 900  
901 Scott, R. C., Menendez de la Prida, L., Mahoney, J. M., Kobow, K., Sankar, R., & de Curtis, M. (2018, Aug).  
902 WONOEP APPRAISAL: The many facets of epilepsy networks. *Epilepsia*, 59(8), 1475-1483.  
903 <https://doi.org/10.1111/epi.14503>
- 904  
905 Shannon, C. E. (1948). A Mathematical Theory of Communication. *Bell System Technical Journal*, 27(3),  
906 379-423. <https://doi.org/10.1002/j.1538-7305.1948.tb01338.x>
- 907  
908 Suarez, L. M., Cid, E., Gal, B., Inostroza, M., Brotons-Mas, J. R., Gomez-Dominguez, D., de la Prida, L. M.,  
909 & Solis, J. M. (2012). Systemic injection of kainic acid differently affects LTP magnitude  
910 depending on its epileptogenic efficiency. *PLoS One*, 7(10), e48128.  
911 <https://doi.org/10.1371/journal.pone.0048128>
- 912  
913 Tatum, W. O. t. (2012, Oct). Mesial temporal lobe epilepsy. *J Clin Neurophysiol*, 29(5), 356-365.  
914 <https://doi.org/10.1097/WNP.0b013e31826b3ab7>
- 915

- 916 Valero, M., Averkin, R. G., Fernandez-Lamo, I., Aguilar, J., Lopez-Pigozzi, D., Brotons-Mas, J. R., Cid, E.,  
917 Tamas, G., & Menendez de la Prida, L. (2017, Jun 21). Mechanisms for Selective Single-Cell  
918 Reactivation during Offline Sharp-Wave Ripples and Their Distortion by Fast Ripples. *Neuron*,  
919 94(6), 1234-1247 e1237. <https://doi.org/10.1016/j.neuron.2017.05.032>
- 920  
921 Van de Ville, D., Britz, J., & Michel, C. M. (2010, Oct 19). EEG microstate sequences in healthy humans at  
922 rest reveal scale-free dynamics. *Proc Natl Acad Sci U S A*, 107(42), 18179-18184.  
923 <https://doi.org/10.1073/pnas.1007841107>
- 924  
925 Wibrál, M., Lizier, J. T., Vogler, S., Priesemann, V., & Galuske, R. (2014). Local active information storage  
926 as a tool to understand distributed neural information processing. *Front Neuroinform*, 8, 1.  
927 <https://doi.org/10.3389/fninf.2014.00001>
- 928  
929 Wibrál, M., Priesemann, V., Kay, J. W., Lizier, J. T., & Phillips, W. A. (2017, Mar). Partial information  
930 decomposition as a unified approach to the specification of neural goal functions. *Brain Cogn*,  
931 112, 25-38. <https://doi.org/10.1016/j.bandc.2015.09.004>
- 932  
933 Witter, M. P., Griffioen, A. W., Jorritsma-Byham, B., & Krijnen, J. L. M. (1988). Entorhinal projections to  
934 the hippocampal CA1 region in the rat: An underestimated pathway. *Neuroscience Letters*,  
935 85(2), 193-198. [https://doi.org/10.1016/0304-3940\(88\)90350-3](https://doi.org/10.1016/0304-3940(88)90350-3)
- 936  
937 Witter, M. P., Groenewegen, H. J., Lopes da Silva, F. H., & Lohman, A. H. M. (1989). Functional  
938 organization of the extrinsic and intrinsic circuitry of the parahippocampal region. *Progress in*  
939 *Neurobiology*, 33(3), 161-253. [https://doi.org/10.1016/0301-0082\(89\)90009-9](https://doi.org/10.1016/0301-0082(89)90009-9)

940

## 941 [Acknowledgements](#)

942 P.P.Q. and A.G. performed and administered all surgery, implantation, and experimental  
943 recordings. P.P.Q. performed spike sorting, spectral analysis, and data pre-processing. W.C. and  
944 D.B. performed computational analysis. T.M. assisted with computational analysis and many of  
945 the supplementary materials. All authors designed the study and wrote the manuscript. W.C. is  
946 funded through the M-GATE program, who has received funding from the European  
947 Union's Horizon 2020 research and innovation program under the Marie Skłodowska-Curie  
948 grant agreement No 765549. T.M. was funded through Aix-Marseille Université. P.P.Q.  
949 acknowledges support from FRM, FFRE and CURE Epilepsy Taking Flight Award. D.B. has

950 benefitted for this work from support provided by the French Agence Nationale pour la  
951 Recherche (ERMUNDY, ANR-18-CE37-0014-02) and by the University of Strasbourg Institute for  
952 Advanced Study (USIAS) for a Fellowship, within the French national programme “Investment  
953 for the future” (IdEx-Unistra). C.B. is funded through ANR 19-CE14-0036-01. The funders had no  
954 role in study design, data collection and analysis, decision to publish, or preparation of the  
955 manuscript. The authors would like to thank Romain Goutagny and Anna Levina for scientific  
956 discussions and comments regarding this work.

957

#### 958 [Data Availability](#)

959 Partial data and codes can be found here: [10.5281/zenodo.4534369](https://zenodo.org/record/4534369)

960 Full codes, including figure generation as well as complete dataset are available upon request.

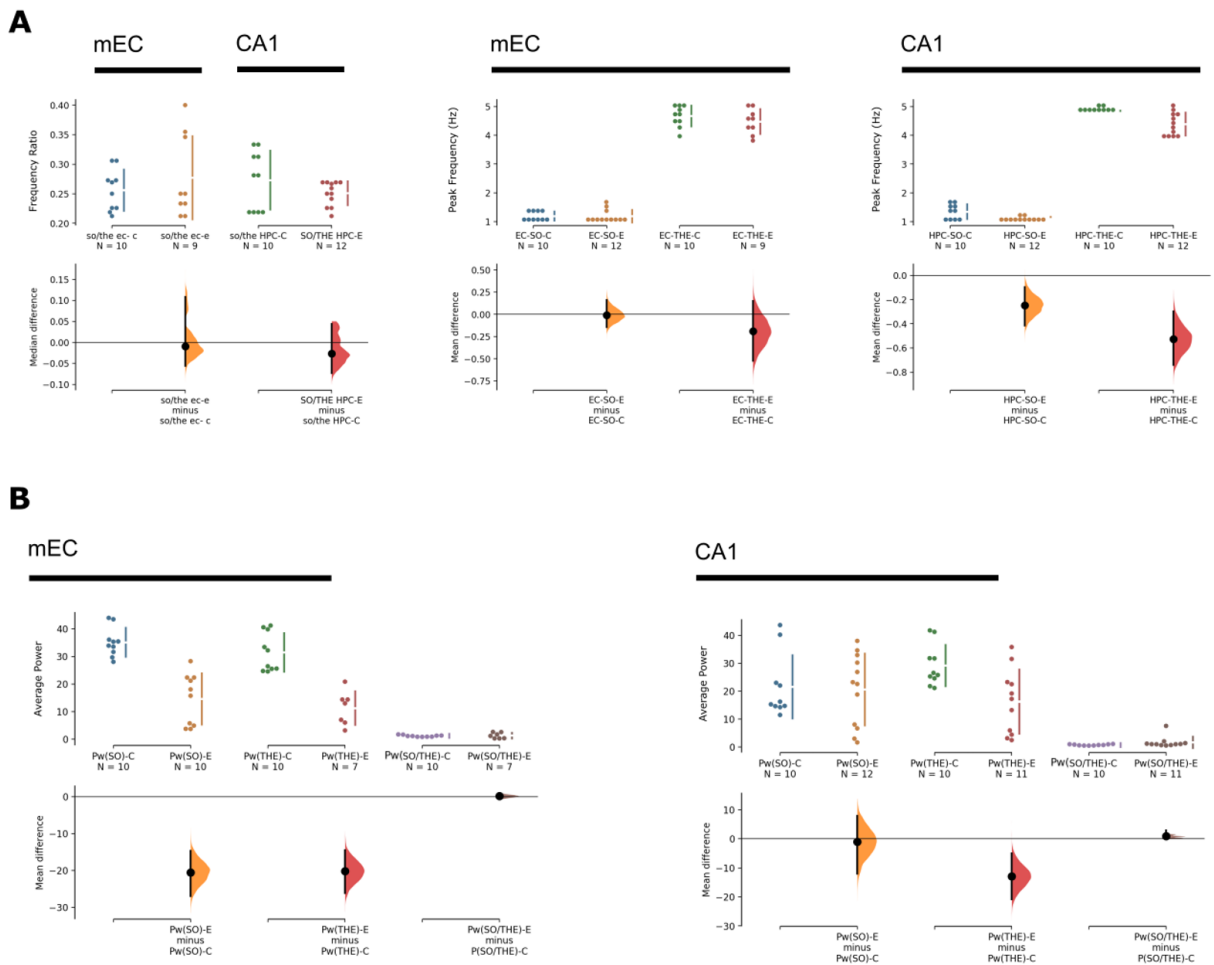
961

#### 962 [Competing Interests](#)

963 The authors declare that they have no competing interests.



964 **Supplementary Figures**



965

966 **S1 – Frequency and Power Relationships in mEC and CA1 in control and epilepsy conditions –**

967 **(A)** (Far Left) A comparison of ratios between peak frequencies during periods of SO and THE in

968 both control and epileptic conditions for mEC and CA1. (Middle and Right) Peak frequencies

969 used in the previous graph for periods of SO and THE in control and epilepsy for mEC and CA1.

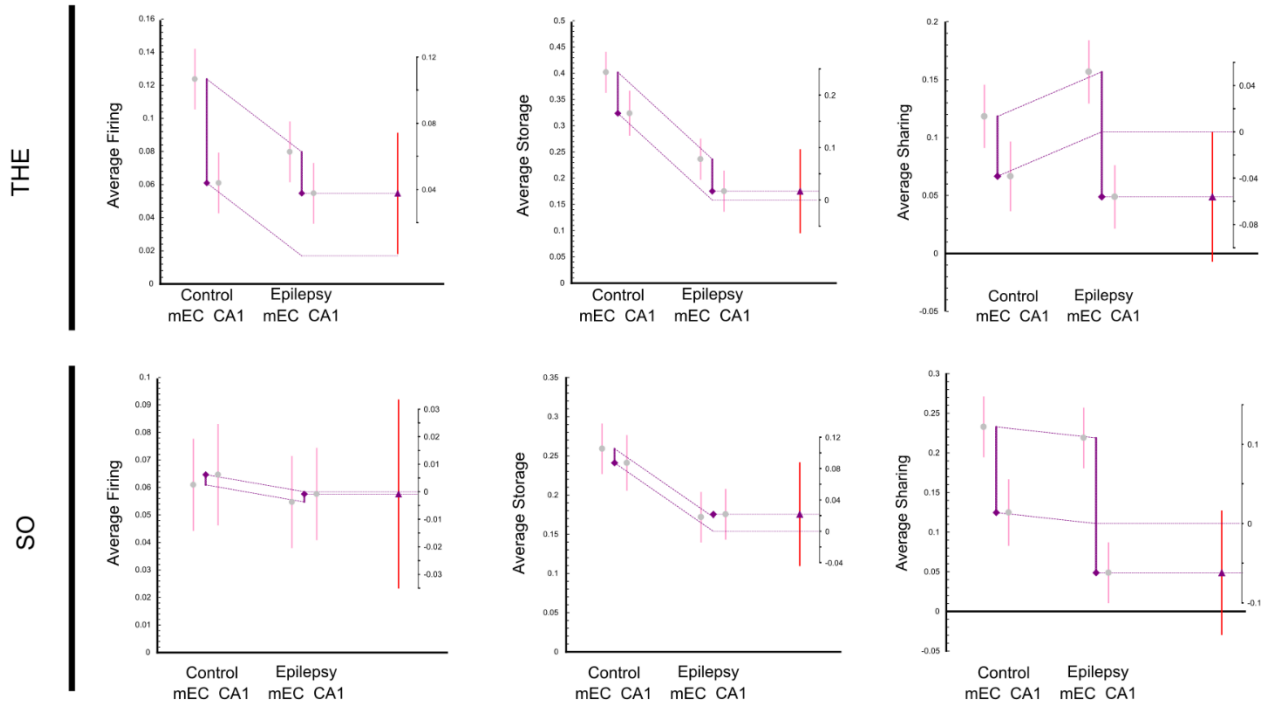
970 There was a strong and smaller effect size on THE and SO peak frequency in CA1 in TLE,

971 respectively. In these Cumming estimation plots, circles represent the mean, and all bars

972 represent a 99% bootstrapped confidence interval. **(B)** The average power found in periods of

973 SO and THE shown next to their ratio for both mEC and CA1. Note the strong effect size on THE

974 and SO power in the mEC, and to a lesser extent on THE power in CA1. For all graphs, 5000  
975 bootstrap samples were taken; the confidence interval is bias-corrected and accelerated.



976

977

978

979

980

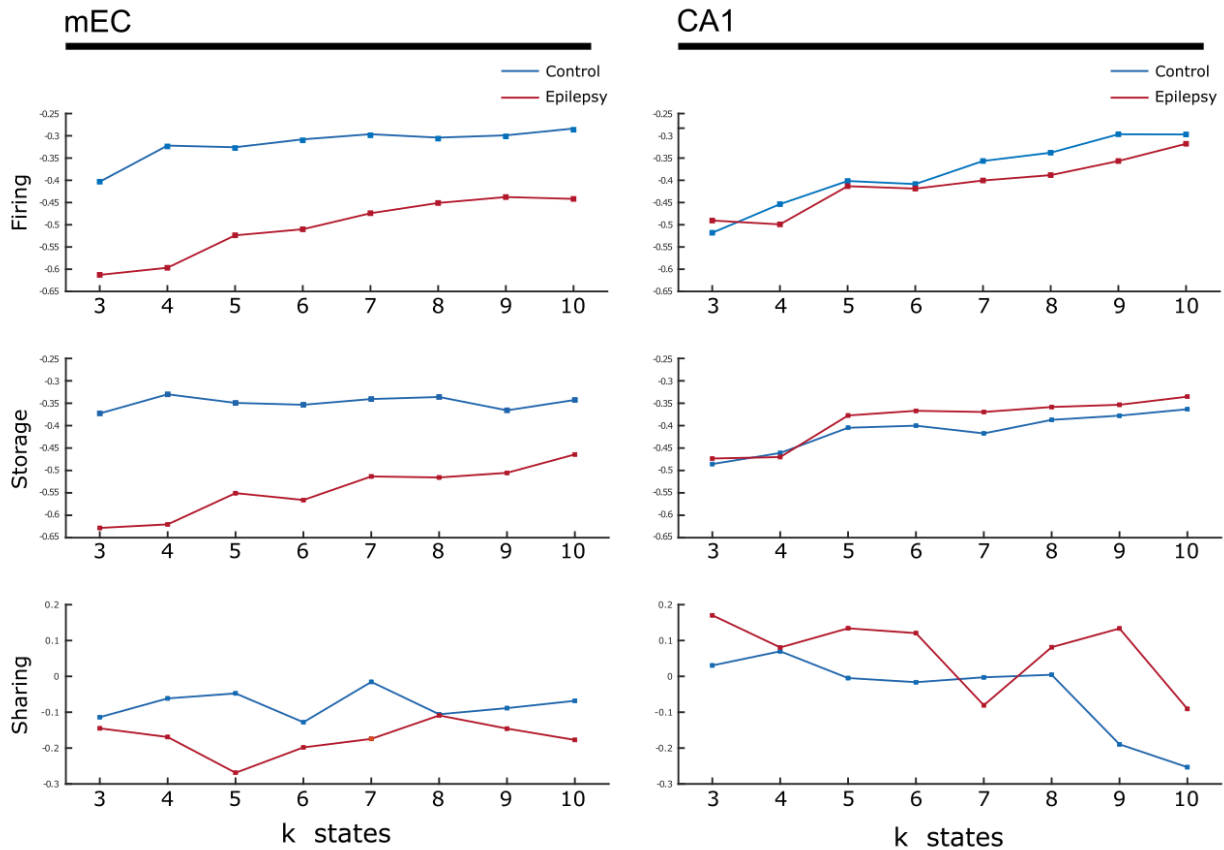
981

982

983

**S2 – Average feature values presented as a function of mEC and CA1 in control and epilepsy conditions** – The same graph as Figure 1D presented in an alternate format to highlight regional differences in control and epilepsy. The differences between mEC and CA1 during THE and SO are similar in control and epilepsy for average firing and average storage. The difference tends to increase for average sharing, but the effect size is consistent. Circles and triangles represent the mean, and all bars represent a 99% bootstrapped confidence interval.

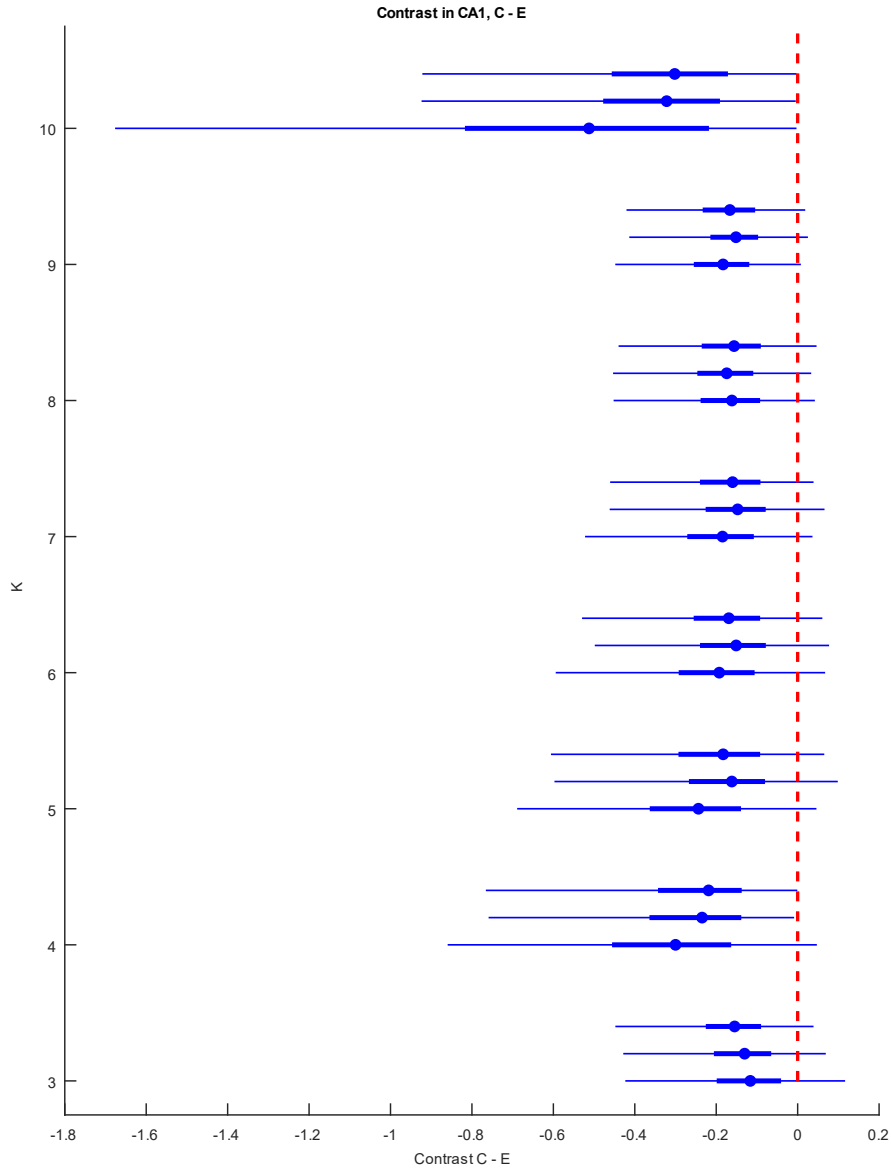
## Silhouette Difference



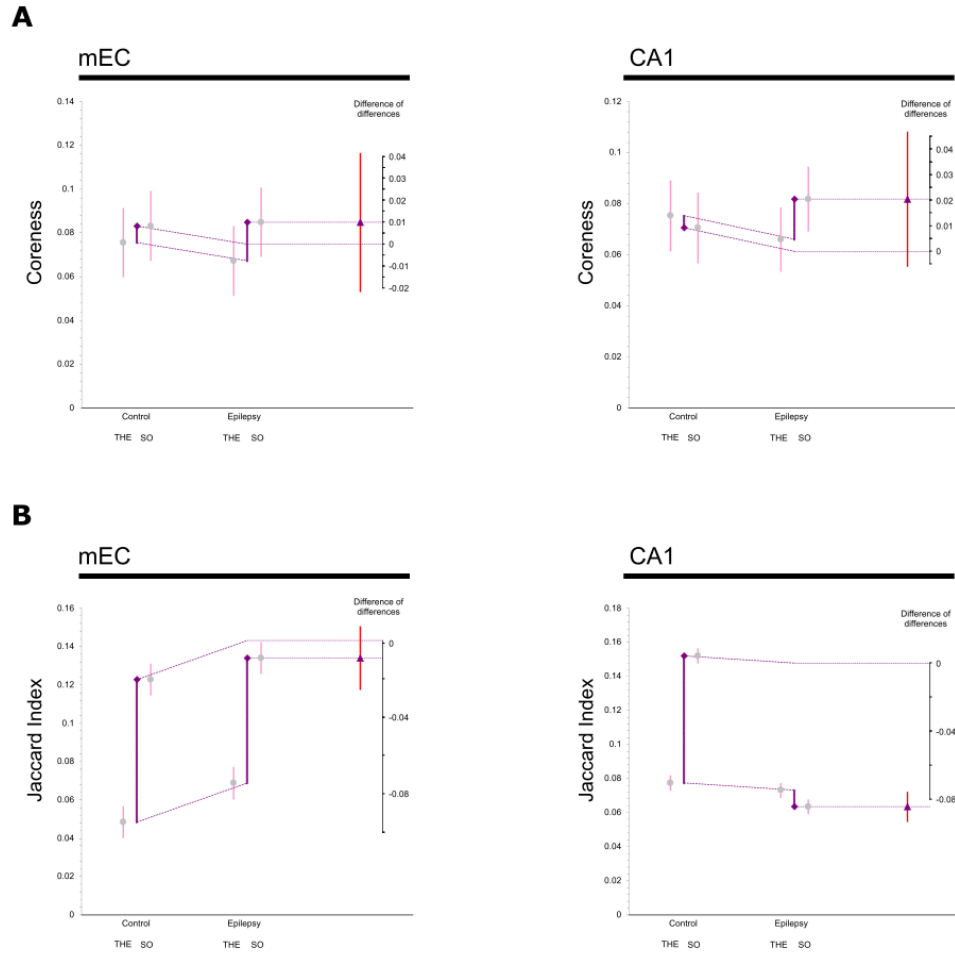
984

985 **S3 – Null model with mean silhouette difference** – The mean silhouette difference between a  
986 randomized null clustering model and the silhouettes found using k-means on non-shuffled  
987 data. Each point was calculated by computing mean silhouette values from a random selection  
988 of the randomized and normal clustering and taking the difference. This was done 500 times to  
989 produce error bars, but the error bars were so small that they appear to be squares on the  
990 graph. The blue line is representative of control data and the red line represents epilepsy data.  
991 There is a very large difference for firing and storage modalities from the null model for all  $k$   
992 values in both CA1 and mEC in control and epilepsy conditions. Of special note is the sharing  
993 states found within CA1 (bottom right). We find that for both control and epilepsy conditions,

994 our measure crosses 0 at  $k=5$  and  $k=7$ , respectively, but fluctuates back above 0 until  $k=9$  states  
995 in control and  $k=10$  in epilepsy. This would indicate that the clustering only weakly holds in  
996 these intermediate values of  $k$  before not separating states better than a null, shuffled model  
997 up until the higher  $k$  values. Therefore, it may be that the states are either less definable in CA1  
998 or, that on average there tend to be more states for sharing in both the control and epileptic  
999 states in CA1 and would therefore require higher  $k$ , on average.



1000 **S4 – Contrast Values for Control vs Epilepsy in CA1** – Average contrast difference between  
1001 control and epilepsy is shown with respect to both feature and number of states,  $k$ . The circles  
1002 represent the mean difference, the thick blue bars represent the 25-75% quantile and the thin  
1003 blue bars represent the 1-99% quantile. The red dotted line is to add the null hypothesis line of  
1004 no significant difference between control and epilepsy.



1005

1006 **S5 – Coreness and Jaccard Values** – Average values and difference of differences graphs for

1007 data features taken from sharing networks, found using the sharing feature, for both

1008 control and epileptic animals. Circles and triangles represent the mean, and all bars

1009 represent a 99% bootstrapped confidence interval. Note the very large effect size in the

1010 decrease of the Jaccard index in CA1 during SO. Accordingly, the brain state specificity of

1011 connectivity variance is lost. Significance is shown using the symbol (\*) with their standard

1012 corresponding meaning (\*,  $p < 0.05$ ; \*\*,  $p < 0.01$ ; \*\*\*,  $p < 0.001$ ).

1013 **ST1 – P value reporting: THE/SO unpaired mean difference**

	mEC			CA1		
<b>Firing</b>	mean difference	CI	P value	mean difference	CI	P value
Control	-0.0593	[-0.0815, -0.0365]	0	-0.0475	[-0.0823, -0.0162]	0.0002
Epilepsy	-0.0217	[-0.0432, -2.55e-05]	0.008	0.00082	[-0.0226, 0.0263]	0.00082
<b>Storage</b>						
Control	-0.133	[-0.18, -0.0859]	0	-0.0828	[-0.146, -0.0214]	0.0002
Epilepsy	-0.0584	[-0.0933, -0.0224]	0	0.0034	[-0.0452, 0.0528]	0.0034
<b>Sharing</b>						
Control	0.109	[0.0643, 0.16]	0	0.0582	[0.0369, 0.0814]	0
Epilepsy	0.0535	[-0.022, 0.128]	0.0594	0.0285	[0.0105, 0.0435]	0

1014

1015 The p-value reported here is from a two-sided permutation t-test with CI intervals at 99%. 5000

1016 bootstrap samples were taken; the confidence interval is bias-corrected and accelerated. The *P*

1017 value(s) reported are the likelihood(s) of observing the effect size(s) if the null hypothesis of

1018 zero difference is true. For each permutation *P* value, 5000 reshuffles of the control and test

1019 labels were performed. They are included here to satisfy a common requirement of scientific

1020 journals. (Ho et al., 2019)



1021 **ST2 – P value reporting: Difference of Difference Graphs**

	mEC			HPC		
	Effect	CI	P value	Effect	CI	P value
<b>Firing</b>						
Control v Epilepsy	-0.025	[-0.043, -0.007]	<0.001	-0.031	[-0.051, -0.011]	<0.001
THE v SO	-0.044	[-0.062, -0.026]	<0.001	-0.023	[-0.044, -0.003]	0.003
Diff of Diff	0.0377	[0.001, 0.0744]	0.008	0.048	[0.0072, 0.0889]	0.002
<b>Storage</b>						
Control v Epilepsy	-0.126	[-0.161, -0.092]	<0.001	-0.107	[-0.147, -0.068]	<0.001
THE v SO	-0.104	[-0.138, -0.069]	<0.001	-0.041	[-0.081, -0.002]	0.007
Diff of Diff	0.0783	[0.0099, 0.1467]	0.003	0.083	[0.0041, 0.1619]	0.007
<b>Sharing</b>						
Control v Epilepsy	0.0122	[-0.032, 0.0563]	0.474	-0.033	[-0.047, -0.018]	<0.001
THE v SO	0.0844	[0.0443, 0.1325]	<0.001	0.0433	[0.029, 0.0576]	<0.001
Diff of Diff	-0.052	[-0.141, 0.0359]	0.126	-0.03	[-0.58, -0.001]	0.007
<b>Coreness</b>						
Control v Epilepsy	-0.003	[-0.019, 0.0124]	0.578	0.001	[-0.012, 0.0143]	0.849
THE v SO	0.0126	[-0.003, 0.0285]	0.04	0.0056	[-0.008, 0.0188]	0.28
Diff of Diff	0.0099	[-0.022, 0.0416]	0.42	0.0205	[-0.006, 0.047]	0.047
<b>Jaccard</b>						
Control v Epilepsy	0.0158	[0.0074, 0.0241]	<0.001	-0.046	[-0.051, -0.042]	<0.001
THE v SO	0.0615	[0.0615, 0.0782]	<0.001	0.0325	[0.028, 0.0369]	<0.001
Diff of Diff	-0.009	[-0.026, 0.0076]	0.16	-0.084	[-0.093, -0.075]	<0.001